Doctoral Dissertation
Doctoral Program in Energy Engineering (35th Cycle)

Development and optimization of fiber bragg grating sensors in geophysical monitoring

By

Aarathy Ezhuthupally Reghuprasad
******

Supervisor
Prof. Alberto Godio, Supervisor

Politecnico di Torino
2023

Declaration

I hereby declare that the contents and organization of this dissertation constitute my own original work , chapter 4 is the already published work of my paper (Reghuprasad et al. 2023) and do not compromise in any way the rights of third parties, including those relating to the security of personal data.

Aarathy Ezhuthupally Reghuprasad

2023

* This dissertation is presented in partial fulfillment of the requirements for **Ph.D. degree** in the Graduate School of Politecnico di Torino (ScuDo).

To the contributors in my field, whose profound impact shaped my research.

To the unwavering dreamers, shaping a brighter world.

To my dearest family and peers, the cornerstone of my journey.

Acknowledgment

I would like to express my deepest gratitude to my supervisor, Prof. Alberto Godio, for his unwavering support, guidance, and expertise throughout the entire research process. His valuable insight, constructive feedback, and dedication to my academic growth have been instrumental in shaping this thesis.

I am immensely grateful to Prof. Davide Luca Janner for his invaluable feedback and suggestions that enhanced the quality of my research.

I extend my sincere appreciation to my doctoral committee members Prof. Carlo Vincenzo Camporeale and Prof. Costantino Manes for their valuable feedback and insightful suggestions during yearly exams.

I am thankful to Prof. Valentina Socco for sharing her expertise in geophysics and being a person of motivation.

I am thankful to Prof. Chiara Colombero for her assistance and support provided during the lab and field experiments. Her technical expertise, availability, and willingness to assist with the experimental setups and data analysis have been crucial in the successful completion of this research.

I thank Dr. Carmine Todaro for providing me with the samples for the experiment. This experiment will not be possible without his help of him with the casting of the samples and sharing his expertise about the material.

I would like to express my gratitude to the Links Foundation for their financial support through the Photo NeXT Scholarship.

I would like to acknowledge the support and assistance provided by the research staff and technicians Diego Franco and Claudio De Regibus from the Department

of Environment, Land and Infrastructure Engineering, Massimiliano Corrado Mattone from the Department of Mechanical and Aerospace Engineering, Alessandro Sanginario from the Department of Electronics and Telecommunications for their expertise, guidance and assistance in the laboratory work have been indispensable in this research endeavour.

I am thankful to my colleagues Andrea, Karim, Farbod, Oscar and Francesca for their stimulating discussions, constructive feedback. Their moral supports during the challenging times of my Ph.D.

I am deeply indebted to my family for their unwavering support, love, and belief in my abilities. To my husband who shared the highest and deepest moments of these years. He has always been with me to calm and happy during the difficult times.

Lastly, I would like to acknowledge my friends and loved ones for their patience and encouragement during the challenging phase of Ph.D.

I am profoundly grateful to all the individuals mentioned above, as well as many others who have contributed in various ways of completion of this thesis.

Contents

List of Figures

List of Tables

Chapter 1

Introduction

1.1 Motivational Background

Geophysics is the application of physics in the investigations of the earth. Further geophysics is subdivided based on the study of different parts of the earth. For example, solid earth geophysics deals with the study of the interior of the earth, applied geophysics is concerned with the investigation of the Earth's crust and near-surface, and engineering geophysics is based on the study of the investigation of subsurface material and structures (M. Reynolds, 1997). In this thesis, we are concerned with engineering geophysics for the application of vibrational analysis and non-destructive test in structural monitoring.

In the past decades all over the world, several natural disasters have occurred. The aftereffects of these disasters are huge, like thousands of victims due to the collapse and damage of the civil engineering structures. Therefore, there is a need for the development of real-time monitoring and early warning of the geohazards to prevent and reduce the loss of life and property.

Since 1930 there has been a tremendous development and usage of geotechnical instrumentation for the investigation of early detection thereby ensuring safety(Zhang et al. 2017). The sensing of these instruments is based on optical, mechanical, and electrical. Another important parameter required for modern geophysical instrumentation is the real-time collection of large amounts of data and high-sensitivity sensors. Electrical based sensors are dominantly used in the market. There are limitations to them being prone to electromagnetic interference and requiring frequent calibration. Due to these limitations, the optical technology based on optical fibers is considered as a promising field for the gathering of data efficiently and sensitivity since light is the signal transferred instead of the electron flow thereby immune to electromagnetic interference (Fenta et al.,2021).

Optical fiber sensor uses the fiber as a sensing element or a path for the signal from the external sensing head. Optical fiber sensing enables the high sensitivity, high data acquisition, fast recording time and high spatial resolution. Fiber optic sensing in geophysics was initially focused on the oil and gas industry for the measurement of pressure, and temperature at single points in the downhole measurement (Silkina 2014). This technology also allows the geophysical community to detect different properties of earth like temperature, pressure, strain, and others with high data sampling. Later studies were done for earthquake detection, mining, geothermal studies, landslide detection, and monitoring of tunnels and bridges.

The most used fiber optic sensing in geophysics is distributed sensing mainly distributed acoustic sensing (DAS)(Shang et al. 2022; Ajo-Franklin et al. 2019), distributed pressure sensing (DPS), distributed strain sensing (DSS) and distributed temperature sensing (DTS) (Ukil et al. 2012; Tyler et al. 2013)are based on the Raman, Brillouin and Rayleigh scattering of light and Fiber Bragg Grating Techniques. Currently with the development of distributed fiber sensing has open a unique opportunity for the geophysics community.

Our focus is on the Fiber bragg grating sensors for the geophysics applications. (Hill and Meltz (1997) demonstrated the formation of gratings (periodic variation in the fiber optic core) in a photosensitive fiber. The sensing principle of fiber bragg grating sensors is when a light is incident on the fiber, a portion of light with a certain intensity is reflected due to the periodic variation in the fiber core. This reflected wavelength is dependent on the periodicity and effective refractive index of the fiber core. A change in the fiber length, due to the physical parameters like strain and temperature, affects the change in the periodicity that results in the change of the reflected wavelength. The change in the reflected wavelength corresponds to the strain and temperature. At the same time, we can also measure other physical parameters like acceleration, pressure, displacement by connecting the FBG into a transducer based on the packaging. The bragg gratings are point sensors that can be multiplexed all the optical Fiber. Based on the application we can use different bragg grating based on the design like standard bragg gratings, long period gratings, tilted bragg gratings, and chirped bragg gratings.

Advantages of fiber bragg gratings in geophysics is their immunity to electro-magnetic interference(EMI), high sensitivity and accuracy to detect small changes which is ideal for the detection of abnormalities and shifts in geophysical systems, small size, multiplexing capability and remote sensing reduces the frequent visit to

the test site and enables a cost effective monitoring of the distributed and large geophysical networks, resistance to corrosion, low heat loss ,resistance to harsh environment (high temperature, high pressure),suitable to deploy for long term, integration with the existing structures (bridges and tunnels) by reducing the installation cost and fitting of the sensors without disruption of these structures in a non-destructive and non-invasive way.

Due to all these advantages of FBGs, there has been an improvement in the ongoing research and advancement in the development of new FBG designs, signal processing algorithms and multiplexing techniques there by enhancing the reliability, performance, and sensitivity of the sensors in geophysics applications.

We should also consider the limitations of this sensors, as they are the quasi-distributed sensors the number of sensors in a fiber is limited based on the demodulation technique. On the other hand, the cost of FBG based system is higher than the conventional sensors. It is predictable to reduce the cost if industrial sectors use the FBG, developing the demodulation system according to our needs and multiplexing many sensors, from all these practices we can significantly decrease the cost.

Overall FBG sensors is a good choice for the monitoring and management of geophysical systems. This system can enhance the safety, performance and real time decision making in the geophysical applications (Fenta, Potter, and Szanyi 2021b),(Riza et al. 2020).

1.2 Problem Identification

This thesis focuses on two distinct problems in the geophysics that need to be addressed to prevent the geohazards and ensuring the safety of the people.

Problem Statement 1:

The deterioration and decay of the materials used in civil engineering infrastructure in the form of corrosion and cracking is one of the main problems faced in the civil engineering. In all these structures the detection of cracking at the early age is important evidence for the damage detection(Safiuddin et al. 2018). The early age cracking is related to the early age shrinkage and creep happening in the material right after the casting. There is a paramount importance for the study on the early age shrinkage for the detection of crack at the early age before reaching

the critical levels, to avoid the failure of structural components or the entire structure.

Presently the most used techniques for the early age crack detection are visual inspections and non-destructive evaluation based on traditional sensors and instrumentations. However, all these techniques are time consuming and inaccurate as they are based on the visual inspections. As a result, there is need for the real time monitoring of the cracks in an accurate and reliable way.

Problem Statement 2:

Seismic instrumentations are used to measure the vibrations within the earth, on the surface of the earth and on the structures like dams and buildings. The importance to measure the vibrations is to prevent the seismic damage and to give the early warning to save the lives and reducing the material losses (Dragomir and Dobre 2021).

Over the past decades there is a significant progress in advancing seismic instrumentation and technologies to achieve high resolution data. Based on field of applications seismic instrumentation requires different sensitivity and the frequency ranges. As the frequency for the earthquakes signals and the structures comes in a different frequency range. Traditional seismic networks have an inherent limited sensing range. As a result, there is a need for the development of seismic network to record the signal in a large bandwidth to avoid the loss of frequency components in the recorded signal and simultaneously record different seismic sources.

In both the problems related to the geophysical structures fiber optic sensing is one of the promising and fastest technology ideals for the assessment of the civil infrastructures from early age and vibration analysis due to its features like small size, non-destructive, multiplexing capability, remote sensing and immune to EMI. Therefore, in this thesis the development of FBG based technique for these two problems are performed to establish them for the future applications.

1.3 Thesis Objective

Based on the problem statements presented, with the production of thesis the following goals and objectives were set out:

1. Perform a detailed literature review on the FBG sensors in geophysics applications to know more about the criticalities faced during the development process.
2. Develop a sensor for the problem statements discussed above. This mainly includes the numerical simulations, optimisation and establishing the system in comparison with the traditional sensors both in the laboratory and the fields. This is done by acquiring, processing and analysing data acquired from both the systems.
3. Explore the applications of the developed sensors in geophysical structures and demonstrate their feasibility of using FBG sensors.

1.4 Thesis Outline

This thesis is divided into five chapters.

In the first chapter, the thesis structure is outlined, initially presented the importance of optical sensing technology for the real time monitoring and early warning for the geohazards to enhance the safety. This is followed by the identification of the problem discussed in this thesis by introducing Fiber Bragg Grating sensors and their role on the geophysical structures. Finally, the objective of the research is outlined and presented.

In the second chapter, a brief introduction and general outline of optical fiber sensors including their classification based on the operating principles and locations are presented. This is followed by the introduction of the Fiber Bragg Grating sensors including the fundamentals, principle, fabrication, and demodulation techniques. Then a general summary about the applications of FBG in the civil structures.

In the third chapter constitutes the centre core of the problem statement 1 for the study on the early age shrinkage in the civil material. The study of the early age shrinkage is done on the two-component grout used for backfilling during tunnel excavations. Initially a brief introduction about the material used and its compositions are discussed. Followed by the design of the FBG sensor, calibration, and packaging of the sensor for the analysis of early age shrinkage and temperature is presented. This is followed by laboratory test of four different samples, data analysis and interpretation. Then a conclusion from the test and results are

showcased presented with the limitations and contributions to the analysis of early detection.

In the fourth chapter, a brief introduction about the seismic instrumentations, optical accelerometers, and fiber bragg grating accelerometers for the development of vibration sensor discussed in the problem statement 2. Further the design, optimisation, fabrication and packing of the sensor is done. Followed by the field test of the developed sensor with the standard vertical sensors for the picking up of the first arrival time of the active seismic sources in the field. Then discussion and conclusion of designed sensor suitable for picking up the first arrival times best for low frequency measurement with high sensitivity is presented.

The final chapter describes the main conclusions obtained through the research performed in the thesis. Along with the future work to continue for the further study.

Chapter 2

Theoretical Background

2.1 Optical Fiber Sensors

In this era of a cyber-physical system comprising of computers, communication, and sensors with the support of data science helps us to make real-time decisions in different applications around us. Here computing and communications systems are much more developed technology in comparison with sensors. There is a critical requirement for sensors as they provide fast and continuous data. By analyzing the data collected from the sensors we can track and monitor the changes that occur in various fields of our life like sensors used in structural health monitoring of bridges and tunnels, condition monitoring of structures in aerospace, medical applications, thermal sensors, motion detection sensors, etc. In all these applications the most effective and promising sensor is the optical fiber sensor.
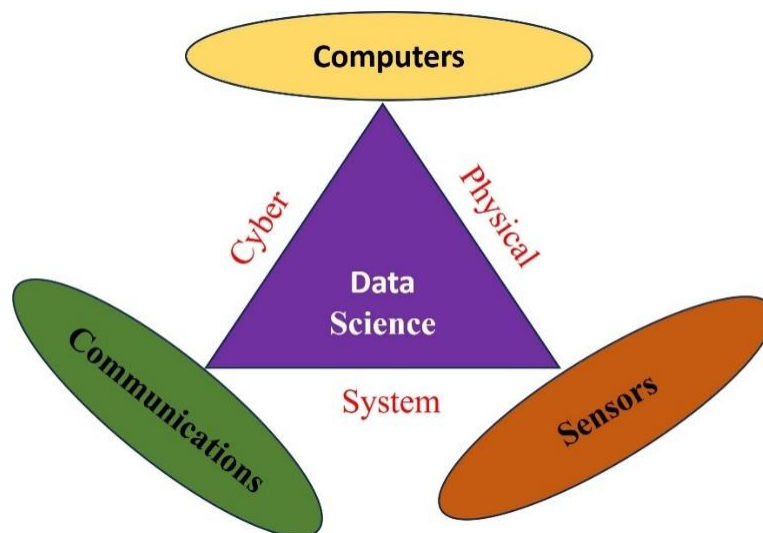
Figure 2. 1 : Schematic diagram of a Cyber Physical System.

Over the past decades, there has been a tremendous improvement in the development of optical fiber sensors (OFS). An OFS utilizes optical fiber as a sensing element or a medium that communicates the signal from an external sensing head. As we know optical fiber is a special kind of optical waveguide that guides light. The optical waveguide effect is achieved by the light carrying fiber core in the center with a refractive index greater than the surrounding cladding which act to traps light in the core. Additionally, a protective coating is applied to safeguard the core and cladding from the potential damage.
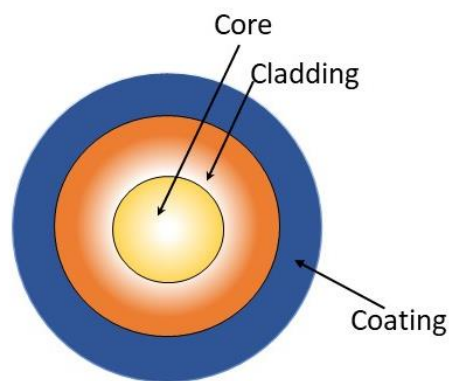
Figure 2. 2 : Structure of Optical fiber cable.

When light moves from one material to another with different refractive index, the beam of light undergoes refraction. When the angle at which the light beam enters the core of the fiber is greater than the critical angle, the light undergoes total internal reflection being reflected into the fiber core without any loss.

OFS is mainly classified into two categories of sensors, mainly extrinsic and intrinsic fiber sensors. In extrinsic fiber sensors, the fiber carries the optical signal to and from where the sensing happens whereas, in the case of intrinsic fiber sensor use fiber as the sensing and the transmitting medium(Fidanboylu and Efendioglu 2009).

The principle of optical fiber sensing is based on modifying of one or more characteristics of the light that passes through the fiber to measure various physical parameters. The parameters considered are the phase, wavelength, polarization, and intensity of light.

$$E(r,t) = a_x E_{0.} \exp[j(\omega t - \beta z)]$$

Perturbation
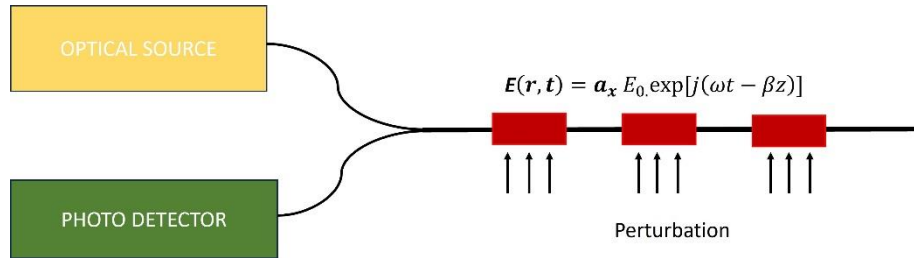
Figure 2. 3 : Typical Configuration of OFS

Compared with electronic sensors they possess advantages like immunity to electromagnetic interference, long-distance sensing capability, small size, multiplexing capability along a single fiber, high sensitivity, low heat loss, chemical corrosion, non-invasive and non-destructive(Sabri et al. 2013).

2.2 Classification of Optical Fiber Sensor

OFS are mainly classified into three categories. They are based on the location of the sensors, operating principle and applications.(Eid 2022).

2.2.1 Operating Principle

Based on the operating principle they can be classified as phase, intensity, wavelength, or a polarization sensor. All these four variables could alter because of disturbances from the external perturbations. Thus, external perturbations can be notified by identifying these parameters and their changes (Kadhum Hisham, 2018).

a. Intensity Modulated Optical Fiber

This sensor uses the intensity of the light to assess the perturbation from the physical parameters. Here, the coupling of the optical fiber with the surrounding medium and micro bending of the optical fiber are changed to alter the intensity of the light going through the fiber. This technique is simple and cheap to construct as it uses a photodetector to measure the intensity of the light transmitted through the fiber and reflected in the input.

b. Phase Modulated Optical Fiber

This sensor is based on phase modulation. They are more sensitive and accurate than the intensity-modulated sensors. Interferometer is used to measure the change in phase. Mach Zehnder, Fabry Perot, Michelson, Sagnac, and grating interferometers are the frequently used ones. Here, coherent light is compared after being split into two pieces and injected into single-mode fibers; one fiber serves as the reference, while the other is subjected to external disturbances that induce a shift and change in the signal's phase. as shown in *Figure 2. 4*.
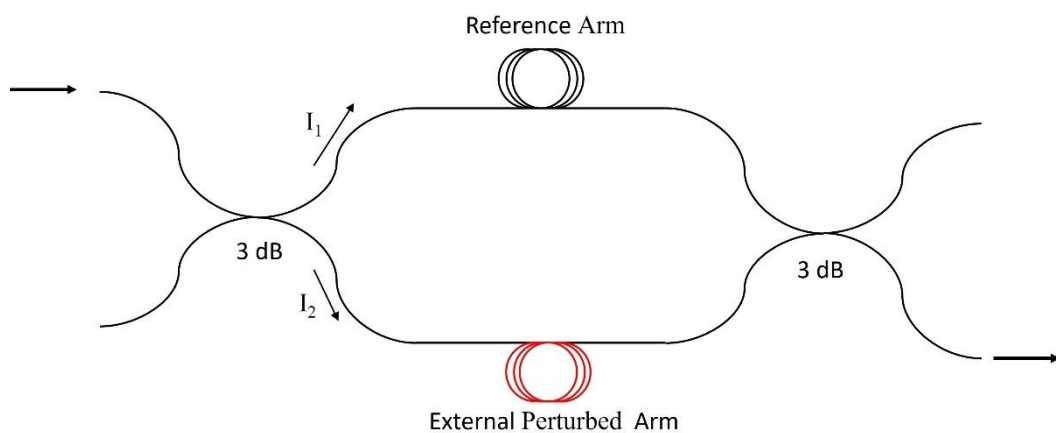
Figure 2. 4 : Phase Modulated OFS

c. Wavelength Modulated Optical Fiber

This sensor is based on the changing in wavelength and frequency of the transmitted light caused by external perturbation. Fiber Bragg Grating sensors are wavelength-modulated sensors. Modifying the refractive index of the core surrounded by the cladding in a periodic manner as shown in *Figure 2. 5*. Based on the bragg diffraction theory this periodic modulation will coherently cause interference for the light in the opposite direction and that light with wavelength λ_B (Bragg wavelength) is reflected

$$\lambda_B = 2\, n_{eff}\Lambda$$
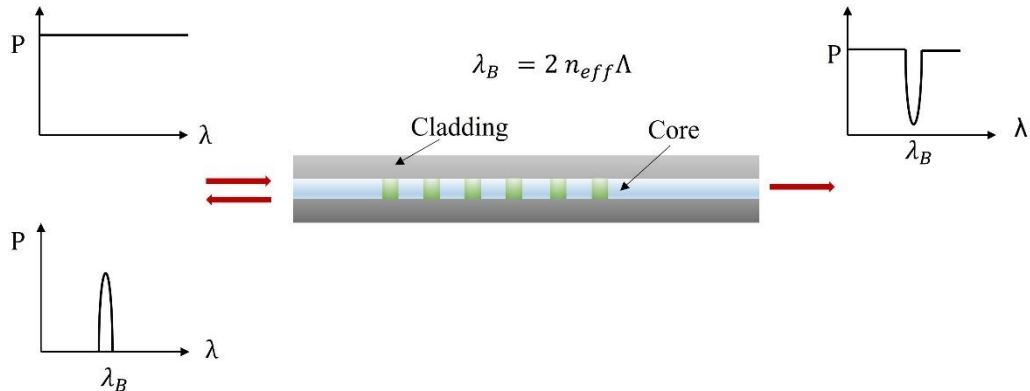
Figure 2. 5 : Wavelength Modulated OFS

d. Polarization-based OFS

Polarization-based OFS utilizes the polarization properties of the propagating light through an optical fiber to measure the physical parameters. The change in the refractive index is caused by an external perturbation like stress or strain, is what drives the operation of polarization-based OFSs. There will be a sizable phase difference because of any change in the refractive index, which will change the polarization orientations. Therefore, by observing the change in polarization, the external disruption can be sensed.

2.2.2 Based on the location.

Generally, the OFS are classified into two types mainly extrinsic and intrinsic OFS. Intrinsic optical fiber the sensing element is the fiber itself and in the case of extrinsic OFS use the fiber as a means of transferring optical signals to and from the location where the sensing is carried out.

There is another classification based on the distribution of OFS along the optical fiber as shown in *Figure 2. 6*.They are divided into three subsets:

a. Single Point: only one sensor in an optical fiber. The measurement variation is detected only in the vicinity of the sensor. However, it is not practical to use many point sensors for the measurement of a larger number of points. This can be solved by multiplexing all the sensing points into an optical fiber. They are mainly used for gas detection and temperature measurement.

b. Quasi Distributed: Multiple sensors in an optical fiber. Here the measurand is monitored at a finite location. Fiber bragg grating sensors are widely used as quasi-distributed sensors.

c. Distributed: OFS are distributed throughout the optical fiber. Raman and Brillouin scattering-based sensors are the widely used distributed sensors. The optical fiber here works simultaneously as the sensing head and transmitting the optical signal. Mainly used in the downhole monitoring in oil/gas exploration, leak detection, geothermal, perimeter sensing, and structural health monitoring of bridges, tunnels, and aeroplanes.
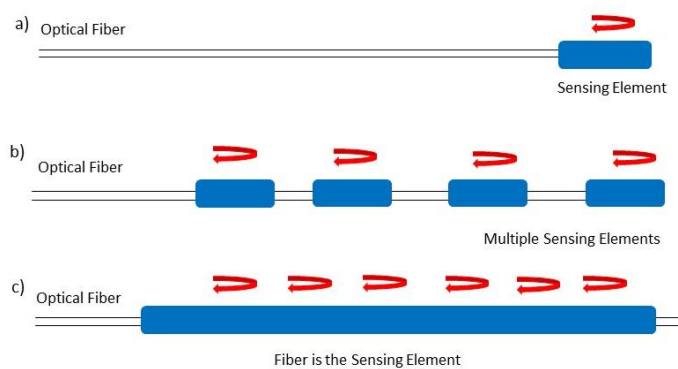
Figure 2. 6 : Schematic Diagram of (a) single Point sensor, (b)Quasi distributed sensor, (c) Distributed sensor.

2.2.3 Based on the applications.

The OFS is classified into three types based on their functioning applications and usage in many sectors.

a. Physical sensor: They are used to measure the physical parameters like strain, temperature, acceleration, force, or other physical quantities. For example, Optical accelerometers, Polarimetric sensors, Fiber bragg grating sensors used for pressure, temperature, and strain measurements, etc.

b. Chemical sensor: They are employed to find the necessary details on the contribution of specific ions or chemicals in a sample. They are used to study the

soil contamination, air pollution, to detect and quantify the presence of specific gas and smoke, pH monitoring in chemical solutions, etc.

c. Bio -medical sensor: These sensors interact with the biological systems, fluids, tissues to provide information for the treatment, diagnosis, and research. They are used for monitoring the blood pressure sensing in body fluids, oxygen monitoring in tissues and blood, etc.

2.3 Fiber Bragg Grating Sensors

(Hill et al. 1978) reported the formation of gratings in a germanosilicate optical fiber by the sustained exposure of the core to the interference pattern produced by the propagating modes of argon-ion laser radiation. Later (Meltz et al., 1989) established the in-fiber grating sensors for writing the fiber bragg gratings directly in the core using a holographic interferometer technique illuminated with a coherent UV source. The versatility of inscribing the gratings increased the interest in the research on fiber bragg grating in the subsequent years. FBG has become a passive device for applications in a fiber laser, optical telecommunications, dispersion compensators, and sensing applications for the measurement of physical quantities in a quasi-distributed manner.

$$\lambda_B = 2\, n_{eff}\Lambda$$
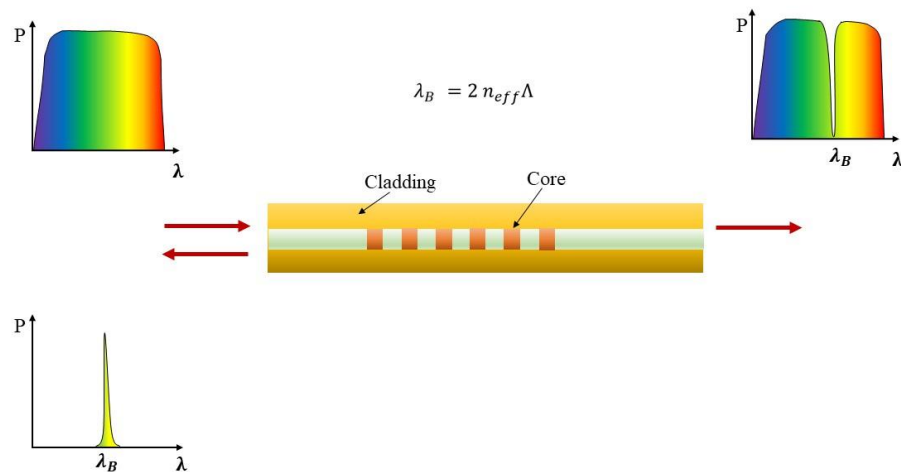
Figure 2. 7 : Schematic diagram of FBG sensors.

These gratings couple light of a particular wavelength from a forward propagating wave to a reflected propagating wave. These grating structures can vary based on the design configuration as shown in *Figure 2. 8*. A standard fiber bragg grating has a uniform grating with a refractive index and the period of modulation as a constant with positive index variation. They typically have sub-micron periods. A long period grating (LPG) has the periods ranging from 100 μm to 1 mm with the principle of operation of coupling the forward propagating core mode with one or more forward propagating cladding modes (Bhatia and Vengsarkar 1996). Since they involve the cladding modes are most affected by the local environment. Chirped Grating the refractive index is a constant with a linear variation in the grating period. The reflection spectrum is wide, and each wavelength component is reflected at different positions resulting in the time delay for different wavelengths(Tosi 2018). Tilted bragg gratings have variation of refractive index is not along the optical axis, whereas it has a certain angle to it. They couple the forward propagating core mode to the backward propagating core mode and a backward propagating cladding mode(Albert et al. 2013; Dong et al. 2011). All these types of gratings can be utilized for different applications.
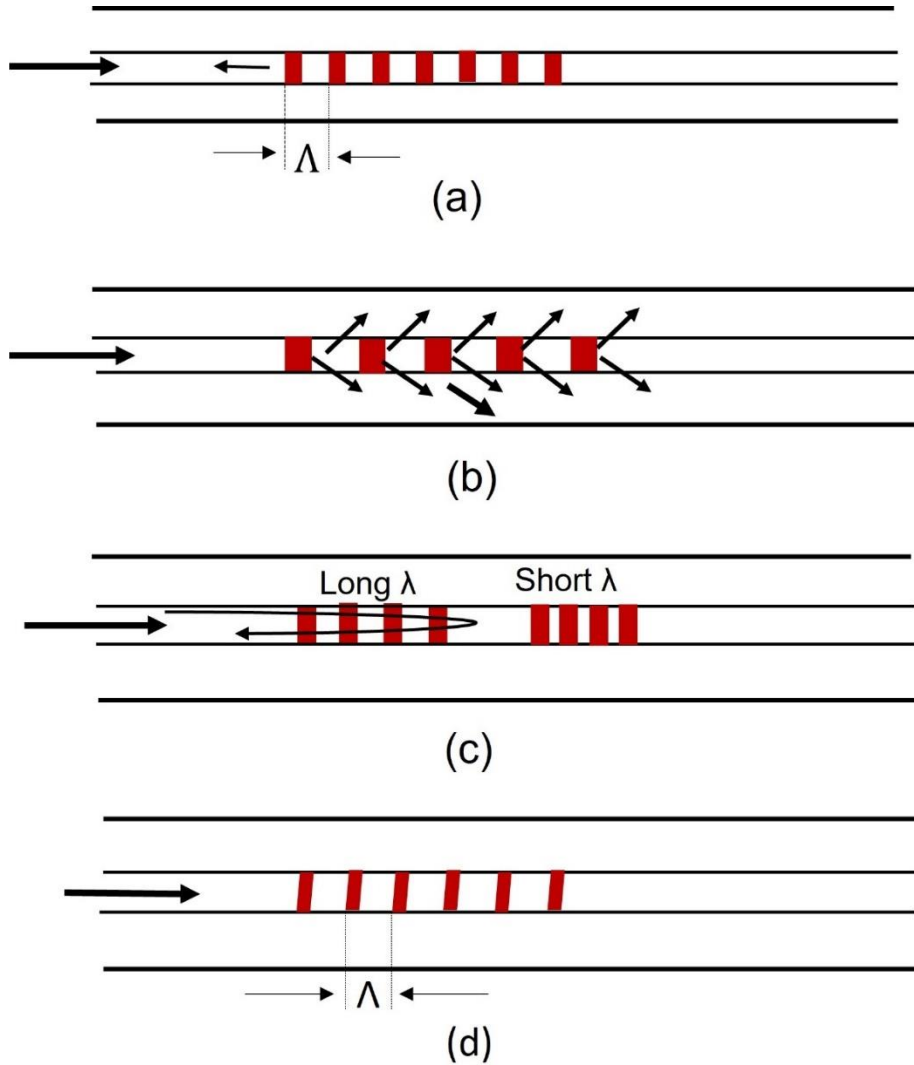
Figure 2. 8 : Different bragg grating configurations. (a) Fiber Bragg Gratings, (b) Long period gratings, (c) chirped fiber bragg gratings, (d) tilted fiber bragg gratings.

In the case of FBG, the wavelength reflected by this intra core gratings is called the Bragg wavelength which is defined by the period of refractive index modulation as given in the equation (2.1):

$$\lambda_B \ (\varepsilon, T) = 2 \ n_{eff} \Lambda \qquad\qquad [2.1]$$

Where, n_{eff} is the effective refractive index of the fiber core and Λ is the grating period (Pendão and Silva 2022).From the Equation (2.1), it can be noticed

that the bragg wavelength is dependent on the effective refractive index and the grating period. This can be affected by both strain and temperature variation.

For the relative strain and temperature variation equation of the bragg wavelength is given in equation (2.2),

$$\frac{\lambda_B\ (\varepsilon, T)}{\lambda_{B0}} = K\varepsilon + \varsigma T \qquad\qquad [2.2]$$

Where, λ_{B0} is the initial bragg wavelength at the start of the measurement, K is the strain sensitivity factor depending the strain optic coefficient, ς is the thermal sensitivity depending on the thermo optic coefficient. Typical strain sensitivity and thermal sensitivity of FBG in an operation wavelength of 1500-1600 nm is 1.2 pm/$\mu\varepsilon$ and 10pm/^{0}C respectively.

As discussed above the FBG sensors are sensitive both to the strain and temperature. So, their effects need to be separated from each other to measure them separately and simultaneously. Research is done on the study of discrimination of strain and temperature. One of the straight approaches is to use a reference grating which is isolated from one parameter for example strain is placed near to the other sensor in the same environment. Another method is to use FBG written on different diameter fibres which gives different strain responses, but the temperature measurement remains the same. The use of two FBGs with different bragg wavelength is also another approach as it shows different responses to the same measurands.

The advantages, disadvantages, and sensitivity of FBG sensors with respect to the other technologies are summarized in the *Table 2. 1* below:

Table 2. 1 : Comparison of different sensing technologies

Sensing Technology	Advantages	Disadvantages	Responsivity/Sensitivity
Fiber Bragg Grating Sensors	• Multiplexing (Many sensors on a single fiber) • Small Size (Compact	• Temperature Cross Sensitivity – Can be solved with packaging	• Typical strain sensitivity and thermal sensitivity of FBG in a

	and lightweight) • Immune to Electromagnetic Interference : No interference from electromagnetic fields • Chemically Inert • High Sensitivity • Can be used in harsh environment	of the FBG sensors for the strain and temperature measurements. • Initial set up cost can be high. • Complexity of the measurement equipment: Interrogator • Sensors are Fragile: Vulnerable to mechanical and optical damage	operation wavelength of 1500-1600 nm is 1.2 pm/$\mu\varepsilon$ and 10 pm/^{0}C respectively. • Suitable for static and dynamic measurements. • Resolution: Sub micron level.
Strain Gauges	• Low Cost - compared to the optical sensors. • Easy to install and use -They can be attached to the surface using adhesive bonding, welding, or soldering. • Accurate and reliable to measure strains from micro to	• Temperature Sensitivity: requires temperature compensations. • Intrusive and Invasive: Can alter the geometry and property of the material. • Susceptible to interference	• Gauge Factor (sensitivity to strain) of the metallic strain gauges is 2. • Semiconductor strain gauges have higher sensitivity. • The actual sensitivity of the strain gauge varies based on the material properties, design, and manufacturing.

	macro levels in static or dynamic situations in different locations or directions in the material.	and errors due to the change in resistance due to the temperature or humidity. • Limited to measure strain on the surface of the material	
Piezoelectric sensors	• It offers a broad dynamic range. • Can withstand harsh environment. • There is no requirement of input power	• Temperature sensitivity • Sensitive to multiple parameters	• The sensitivity varies based on the material property, design and the applications. • Piezoelectric strain sensors have sensitivity varies from microvolts to millivolts per microstrain. • Piezoelectric force sensors have sensitivity in the range from microvolts to millivolts per Newton. • Piezoelectric pressure

			• sensors have the sensitivity in the range from few microvolts to millivolts per pascal. • Piezoelectric acceleration sensors have the range from mV/g to several hundred mV/g • High frequency response
Capacitive sensor	• No contact measurement. • Suitable for dynamic measurements. • High sensitivity	• Susceptible to temperature and humidity • Non-linear behaviour in large displacements. • Cost can be higher compared to other sensors.	• Detection range of 2mm to 50mm
Optical Interferometers	• No contact measurement. • High dynamic range.	• Requires careful alignment. • Vibration sensitive	• The sensitivity depends on the interferometric technique which is

	• High precision • High resolution.	• Complexity in setting up • Cost can be higher compared to other sensors.	based on the application.

Interrogators and demodulators are required to acquire the data from the light signals coming from the FBG sensors. Interrogators are mainly encoded for the bragg wavelength change, so they typically read the change in the wavelength.

2.3.1 FBG Fabrication Technique

FBG sensors are inscribed using the germanium doped silica a photosensitive material whose refractive index can be changed by exposing into the ultraviolet light typically from a Krypton fluoride (KrF)excimer laser at 248 nm or argon ion laser at 244 nm. Absorption of the UV light in the germanium doped fiber causes the permanent refractive index variation. The gratings are inscribed mainly by three methods: Holographic, phase mask and point by point technique(Dewra and Grover 2015).

a) Holographic Interference Technique:

A single UV laser beam is split into two and recombined to form an interference pattern. This method requires a UV source with good temporal and spatial coherence. The advantage of this method is the flexibility to change the bragg wavelength rapidly. Major disadvantage of this system is they require a high mechanical stability and isolation from the vibration to maintain the fringe contrast. They are also highly sensitive to the optical alignment of the system. This method cannot be used for inscribing the chirped bragg gratings.
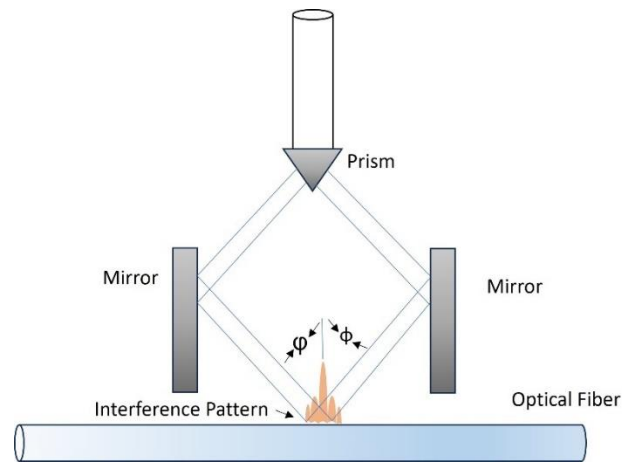
Figure 2. 9 : Holographic Method

b) Phase Mask Technique:

Phase Mask Technique utilizes a diffraction grating to split the single laser beam into different diffraction orders. The formed diffraction orders create the required pattern on the fiber. This method is easy to implement and less sensitive to the vibration and alignment but does not have the flexibility to change the bragg wavelength rapidly. With this method the fabrication cost can be reduced, since several gratings can be printed in a single exposure and requires a low coherence source making it suitable for the production in a bulk. Chirped gratings can be inscribed using this technique.
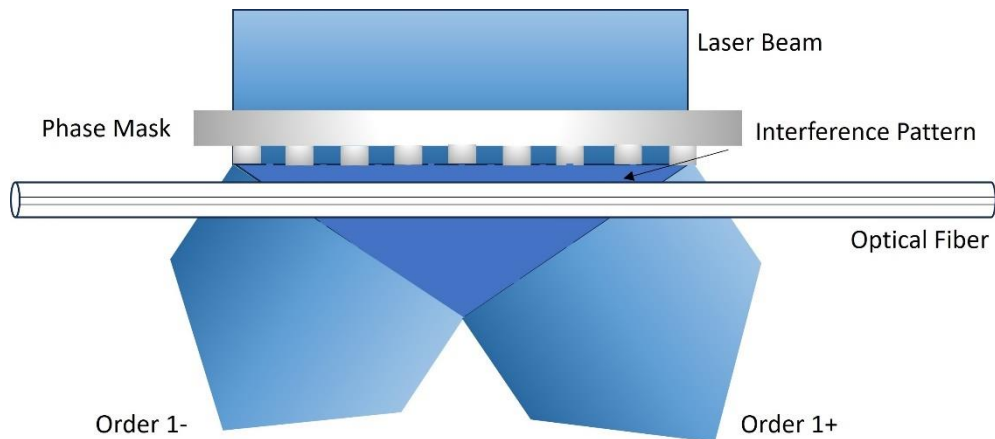
Figure 2. 10 : Phase Mask Technique.

c) Point by Point Technique

   In this technique a pulse of femtosecond laser is used to write the grating point by point. The periodic bragg gratings are created by pulling the fiber along its axis relative to the focused beam of a femtosecond laser falling on the slit with the help of a cylindrical lens. The advantage of this technique is flexibility to fabricate the bragg wavelength with different period.
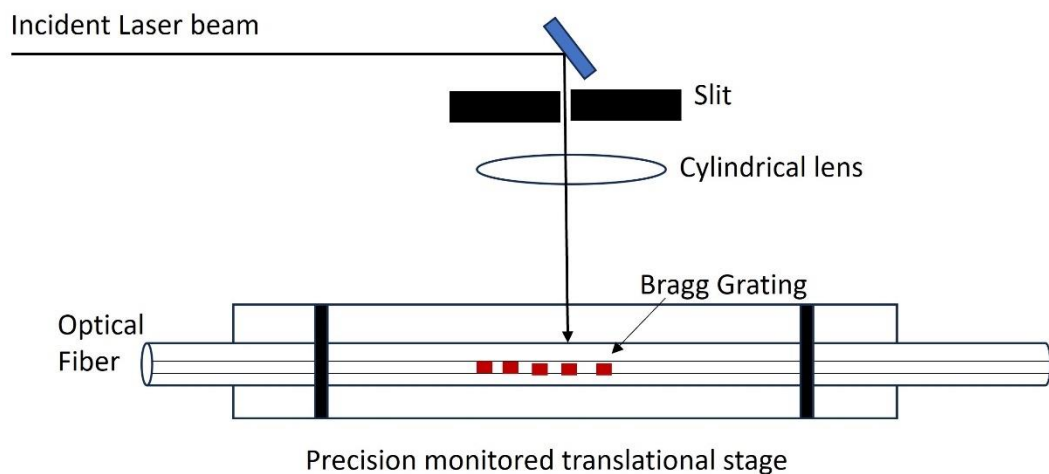
Figure 2. 11 : Point by Point Technique

2.3.2 FBG demodulation

Interrogators and demodulators are required to acquire the data from the light signals coming from the FBG sensors. The primary obstacle for the widespread use of the FBG sensors is the FBG demodulation technology due to the higher cost of the system, which has grown into a significant research area in the past decades for the development of less expensive systems. For detecting the wavelength shift of the fiber bragg grating, there are wide range of demodulation methods, and they are classified into following categories(Chen et al. 2011; Doyle 2003):

a) Interference interrogation methods: In this method the bragg wavelength shift of FBG is converted by interference interrogation into the phase variation of the interferometers like Michelson, Mach Zehnder and Sagnac. Here the variation of the light intensity is measured as the variation of the path difference in the interferometer. These interrogators are potential for higher sensitivity, but they are expensive due to the equipment within the system and susceptible to the disturbance from the environment.

b) Tunable filter: In this technique the reflection wavelength can be identified with the use of narrow band tunable filters like Fabry Perot filter, FBG based optical filter, etc. They are sensitive to the intensity fluctuations in the sensing signal. The limitation of this system is they are not suitable for the fast and dynamic interrogation.

c) Wavelength division multiplexing: This technique is a widely used approach for the interrogation. This system consists either of a broadband light source and a spectrometer for the detection or a simple photo detector and a swept wavelength light source. In this interrogator many gratings with different bragg wavelength can be multiplexed in a

single fiber and address simultaneously. They have high sensitivity and accuracy, flexible to connect many sensors and are relatively large.

d) Time division multiplexing: In TDM uses a pulsed broadband light sources and different gratings are identified based on the time taken for the returned signal to reach the detector. They are low cost, high sampling rate, small and robust. One of the major limitations of this system is the sensors should be placed far from the adjacent sensor.

2.4 FBG Applications in Civil and Environment

1. Structural Health Monitoring

Civil structures are generally large and serve for a very long time. So, it is difficult to judge the positions where damages can take place. To assure the monitoring of these infrastructure we need to install the sensors as many as possible. Due to the multiplexing capability and non-destructive nature of the FBG sensors, they are a promising sensor for the structural health monitoring of these structure. This monitoring helps to prevent failure, increase the safety of the structure and maintenance cost is optimized.

2.Monitoring of bridges

FBG sensors are used as embedded sensors in bridges to monitor strain, displacement, and temperature variations. They monitor the structural response under normal and dynamic loads continuously, which helps to assess the structural integrity, load carrying capability. Sensors are used for monitoring the different phases of the life cycle of bridge from construction to rehabilitation and on various structural components.

3.Monitoring of Tunnels

FBG sensors are installed in tunnels for the measurement of strain and temperature variation. They monitor the behaviour of tunnels during the construction, maintenance phase and operational phase. Even there are studies done on the study of the early age analysis of the concrete used for tunnelling purposes. This study helps us to ensure the safety of tunnel by detecting the deformations.

4.Pipeline Monitoring

FBG sensors are used in oil and gas exploration. They generally measure the strain, temperature, and pressure variations along the pipeline for the detection of leakage. This helps us to improve the structural integrity of the pipeline, prevent leakage.

5.Seismic Monitoring

FBG accelerometers are used to measure the ground vibrations during the earthquakes and seismic events. They assess the seismic performances of structures and evaluate the impact on the structure and safety.

Chapter 3

Static Monitoring

3.1 Introduction

Static monitoring is an early assessment method that can offer a preliminary assessment of the condition of the structure. It involves the continuous or periodic measurement and analysis of various parameters characterizing the behaviours and condition deformation, like by accessing the integrity of the structure, performance and safety of a building, dam, tunnel, bridges, or any kind of infrastructure.

The main advantage of static monitoring is early detection of structural issues, identify the potential risk, implementing the appropriate maintenance and repair. This is mainly done using the sensors, instruments, and data acquisition system for collecting data related to the parameters like deformation, stress, strain, displacement, temperature. The commonly used sensors are the strain gauges, displacement transducers, temperature sensors, tiltmeters and fiber optic sensors.

This chapter deals with the static monitoring of tunnels at the early age by measuring the temperature and shrinkage using fiber optic sensors. This is done to analyse the behaviour and performance of the tunnel during the construction phase. As we know shrinkage is a time dependent deformation that occurs in all types of concrete. This happens mainly due to the loss of water during the drying phase without any impact on the load. Early age shrinkage and temperature monitoring is important as it helps to understand the excessive shrinkage, thermal gradients that can lead to cracking in the construction phase thereby allows to optimize the cement material, water/cement ratio used for construction process.

Shield machines used for tunnel excavation have increased tremendously mainly metro tunnels, and underwater tunnels due to their fast construction speed and less influence on ground disturbance compared with the traditional tunneling

methods (S. He et al. 2020).During the Tunnel Boring Machine shield (TBM) advancements, an annulus or void is created behind the shield tail. The filling of this annulus is a crucial operation in the mechanized tunneling excavation process. So special care is required during this back filling phase independent of their excavation system. This backfilling method prevents or minimizes the surface settlements thereby ensuring a homogenous, uniform, and immediate contact between the ground and lining, waterproofing of the tunnel and the gasketry.

To achieve the efficient back filling the material used for injection should have the following performance, technical and operational characteristics like:

- instantaneous backfilling to avoid the annulus during the TBM advancements.
- the annulus must be consistently and entirely filled for the linings to be connected to the surrounding ground on a regular basics, regarding the mix's transportability, the system's dependability must be ensured. Therefore, the grout must be built to prevent clogging of the injection pipes, as well as segregation and bleeding of the pumps in relation to the amount of time the grout is transported, as well as the distance from batching to injection.
- After the injection, the material must gel extremely quickly.
- Regarding its physical properties and mechanical behaviour, the material should be homogeneous across the annulus.
- It must be impossible for the injected substance to be removed by the groundwater.

Among the existing alternative material for backfilling in tunneling applications two-component grout is the most widely used because of its better capability to control surface settlements in the short term and fast hardening((Peila et al., 2011). It is typically a super fluid grout whose workability is guaranteed for a long duration from batching to transport and injection. During the injection at the annulus an accelerator admixture is added. This mix begins to gel after the accelerator is added in a short time typically 10 to 12 seconds during which the TBM moves forward by about 10 to 20 mm. This gel begins to develop mechanical strength immediately.

Two-component grout is produced by mixing component A and component B together, component A is a cementitious mix formed of water, cement, bentonite, and retarding /fluidifying agent which is a mortar while component B is an

accelerator agent (produced with sodium silicate) (Todaro et.al, 2022).The bentonites enhances the homogeneity and impermeability of the hardened mixture formed after the gel formation. It helps to decrease the bleeding, enhancing the impermeability It also helps to reduce the bleeding, provides better impermeability to the system by assisting in the gelling process during flow interruptions when the annulus is full and contributes to establishing the thixotropic consistency. The retarding agents prevents the mix from setting thereby ensuring its usability for up to 72 hours after the batching. The fluid mortar experiences a rapid gel formation when the accelerator admixture is added thereby building the mechanical strength. The homogeneity of these gels helps to prevent the segment point loading.

Various research has been done on the role of each ingredient in the two-component grout in the past decades. Dal Negro et al. (2014) explained how the retarding agent ensures the necessary workability. Mesboua et al., (2018) put forward the stability of the component A with respect to the role of bentonite. Further, the influence of bentonite was confirmed from the waterproofing capacity of the hardened grout and the gelation phase by (Peila et.al, 2011). Enrico et al. (2010) investigated on the right choice and dosage of the bentonite. Further (Todaro et.al, 2022b) performed the role of bentonite in the two component grout applications. The elastic properties of the two component grouts at a short curing time was investigated by (Todaro and Pace 2022a).

There is a limited knowledge on the properties of both fresh and hardened grout of the two-component mix. Practically, it is impossible to measure the early age strain of the two-component grout in the initial hours after casting since strain or displacement gauges cannot be attached until a minimum strength has been obtained. Majority of the shrinkage strain in the literature is measured as of the demoulding time.

The goal of this chapter is to have a better understanding of the two-component grout by using the relatively recent technology called fiber bragg gratings. Various studies have been done on the estimation of physical properties of the concrete using different technologies. (Slowik et al. 2004)and later (Wong et al. 2007) have investigated the simultaneous measurement of early age shrinkage and temperature of the cement using FBG sensors. The advantage of fiber bragg grating sensors for the early age analysis(Luo et al. 2013) . multipoint approach of measurement of early age properties was conducted by (Pei et al. 2014) . Previous work has only focused on the early age measurement of the cement paste. There remains a need for the study of the early age measurements for the two-component grout.

The purpose of this study is to investigate the shrinkage and temperature variation of the two-component grout using fiber bragg grating sensors by embedding them inside the casting mould. By preparing special casting mould, the sensors have been embedded inside the two-component grout. Four different bentonites have been used for preparing the two-component grout mix, by using however always the same dosages of ingredients and just replacing the type of bentonite. The early age shrinkage and temperature measurement of the four mix-designs are the outcomes of this research. The proposed technology and the proposed approach are intended to provide an innovative method for providing answers for the assessment of the shrinkage of the two-component grout.

3.2 Methodology

The early age temperature monitoring is important during the casting of concrete structures. Conventionally temperature monitoring can be done using thermocouples with an acceptable accuracy, but the limitation is the sensing in certain locations only. The mechanical and electrical strain gauges for measuring the shrinkage cannot be attached before the mix is hardened, hence this technique also failed to measure the early age shrinkage. There are other techniques like ultrasonic, calorimetric measurement which requires complex and delicate experimental setups. Compared to all these technique fiber bragg grating technology attracted due to their small size, easy of install the sensor before casting, accuracy in measuring the shrinkage right after the casting, immune to emi.

As we know one of the limitations of these sensors are the inability to discriminate between strain and temperature in a single measurement of the Bragg wavelength shift. To overcome this limit there are several techniques have been proposed such as dual-wavelength superimposed gratings, long-period gratings/hybrid Bragg gratings(Srimannarayana et al. 2008), and dual-diameter FBGs(Jiang et al. 2015).

For the investigation of the early age properties of the two-component grout, the dual FBG sensors are taken into consideration for the simultaneous measurement of strain and temperature. For discriminating the temperature measurement, the dual FBG sensors are encapsulated into a capillary tube. Before casting the bare dual FBG and the encapsulated dual FBG sensors are inserted into the casting mould. They are inserted horizontally into the casting mould at a middle position horizontally.

The interrogation system used for the measurement is Micron Optics Si155 interrogator system was used to acquire the data of FBG wavelength shift with a

sampling frequency of 1 kHz. This system can potentially acquire the measurements of hundreds of sensors on four parallel and 160 nm wide optical channels.

3.2.1 Two Component Mix Used

The two-component mix is a cement-based material made up of two fluids, when thoroughly mixed forms a gelled material that starts instantaneously and continuously hardens. The two-component mix design used is reported in *Table 3. 1*

Table 3. 1 : Two Component Mix design used.

	Ingredients	Dosage(kg/m^3)
Component A	Water	853
	Bentonite	30
	Portland Cement CEM I 52,5R	230
	Retarding/fluidifying agent-Mapequick CBS1	3.5
Component B	Accelerator – Mapequick CBS3	81

For the study of the early age shrinkage and temperature measurement, four different types of bentonites were used(Todaro and Pace 2022b).With regard to the use of bentonite ,the difference in the water to cement ratio(w/c) is equal to 10 kg/m^3.In accordance with (ENFARC,2005),the variation of 1.1% in the water dosage has no impact on the w/c and all the tested mixes are considered of having the same w/c. The cement used consists of 95% clinker and 5% of minor constituents, excluding calcium sulphate and additives.

Table 3. 2 describes the name of the mix designs, bentonite pictures, swell index (SWI), and smectite percentage as reported in (Todaro and Pace 2022b). The colour of the material is random, and it is not dependent on the properties of the bentonites, it is a function of the type of clay and the additives, and this is not relevant in our study. The swell index is a factor that describes the ability of the bentonite to swell as it interacts with water. The XRD analysis of the mix were

conducted by (Todaro and Pace 2022a) for the estimation of percentage by weight of smectite.

Table 3. 2 : Details of four different bentonites mix design.

Name of the mix	Bentonite pictures	Smectite content (% by weight)	SWI (ml/g)
B1	B1	92	23
B2	B2	98	13
B3	B3	88	14
B4	B4	72	19.7

3.2.2 Design of the FBG sensor

As the bragg wavelength shift is affected by both the strain and thermal changes in the grating region, hence distinguishing and isolating the response is necessary when simultaneously measuring the shrinkage and temperature. This discrimination of strain and temperature is achieved by using two dual FBG sensors with one of the dual FBG being free and the other dual FBG being packaged inside an encapsulated tube in an identical situation.

The linear equation for these two sensors is given by:

$$\Delta\lambda_{B1}/_{\lambda_{B1}} = k_{\varepsilon 1}\Delta\varepsilon + k_{T1}\Delta T,$$

$$\Delta\lambda_{B2}/_{\lambda_{B2}} = k_{T2}\Delta T$$

[3.1]

Where λ_B denotes the Bragg wavelength, $\Delta\lambda_B$ denotes the change of bragg wavelength, $k_\varepsilon = (1 - p_e)$, $k_T = (\alpha + \xi)$ represents are the photo elastic parameter related to the fiber property(p_e),α and ξ are the thermal expansion coefficient and thermal optic coefficient of the fiber core, strain change $\Delta\varepsilon$, and temperature change ΔT. The strain and temperature sensor is denoted by subscripts 1 and 2 respectively. We can express this equation in the matrix form:

$$\begin{pmatrix} \Delta\lambda_{B1}/_{\lambda_{B1}} \\ \Delta\lambda_{B2}/_{\lambda_{B2}} \end{pmatrix} = \begin{pmatrix} k_{\varepsilon 1} & k_{T1} \\ 0 & k_{T2} \end{pmatrix}\begin{pmatrix} \Delta\varepsilon \\ \Delta T \end{pmatrix} = K \begin{pmatrix} \Delta\varepsilon \\ \Delta T \end{pmatrix}$$

After solving this matrix, we obtain

$$\Delta\varepsilon = \frac{1}{k_{\varepsilon 1}}\left(\frac{\Delta\lambda_{B1}}{\lambda_{B1}}\right) - \frac{k_{T1}}{k_{\varepsilon 1}k_{T2}}\left(\frac{\Delta\lambda_{B2}}{\lambda_{B2}}\right)$$

$$\Delta T = \frac{1}{k_{T2}}\left(\frac{\Delta\lambda_{B2}}{\lambda_{B2}}\right)$$

[3.2]

From these Equation (3.2), we can determine the early age shrinkage and temperature. By considering the following assumptions on the FBG sensors embedded onto the specimen that the slippage and debonding between the fiber and the mix is negligible, ensuing the strain of the mix is directly transferred to the sensors. Hence the strain experienced by the sensor is the actual strain of the mix. The temperature measurement is from the FBG sensor inside the encapsulated tube.

3.2.3 Sensor Calibration

Before embedding the polyimide FBG sensor into the two components mix it is necessary to calibrate the wavelength shift with the change of temperature. In the test, the calibration is done using the encapsulation of the FBG sensor in two different materials of the capillary tube (Mamidi et al. 2014). The thermal conductivity and thermal capability of the material for the capillary tube was considered while selecting the material given in *Table 3. 3*. The material of the capillary tube used is borosilicate glass and stainless steel. Both the tubes are of length 20 cm with an outer diameter of 1 mm and inner diameter of 0.5 mm. Figure 3.1 shows the apparatus and modality for the sensor calibration particularly for the temperature measurement.

Table 3. 3 : Properties of the Encapsulating Material

Encapsulated Material	Diameter (Inner/Outer) mm	Thermal Conductivity(W/m-^{0}C) at 25^{0}C	Thermal capability(^{0}C)
Borosilicate Glass	0.5/1	1.14	500
Stainless Steel	0.5/1	16	1400
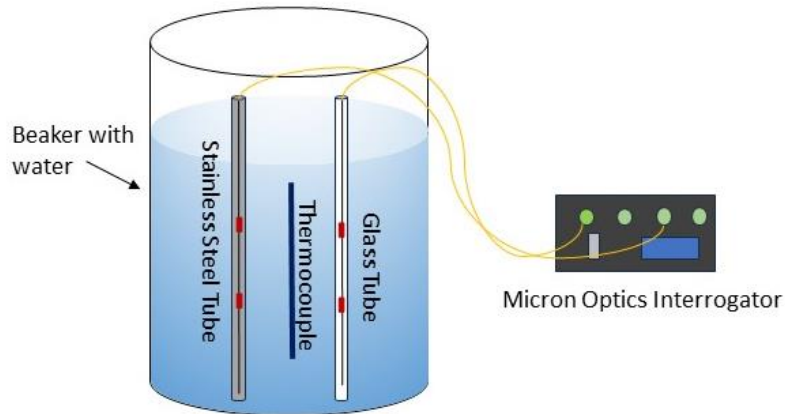
Figure 3. 1 :Schematic diagram of calibration of encapsulated FBG sensor.

The bare FBG sensor is inserted carefully into the capillary tube. For the isolation of induced strain on the FBG due to the thermal expansion of the capillary tube, one end is left free, and the other end fixed. After the encapsulation of the sensors and fixing them into the wall of the beaker with water. The sensor is subjected to the temperature change of water from 20^0C to 60^0C at a step interval of 20 ^{0}C. We have only considered the measurements in three temperatures (20 ^{0}C ,40 ^{0}C and 60 ^{0}C) due to the limitation of controlling the temperature of water in a small interval. So, we repeated the test several times and the shift in bragg wavelength is averaged to determine the sensitivity of the fbg sensors after encapsulation. A thermocouple is also used to monitor the temperature of the water. Both the encapsulated sensors are spliced to the optical patch cord and connected to the Micron Optics Interrogator for data acquisition. Here we have calibrated the sensors for the temperature not for the strain measurement. The test helps us to determine whether borosilicate glass or stainless steel is best   encapsulation tube for our study.

3.2.5 Experimental Setup

The experimental setup, adopted to test the reliability of FBG sensors for measuring strain and temperature of the mixture, is depicted in *Figure 3. 2* .The apparatus is compounded by:

1.Interrogator: Micron Optics Interrogation unit is used for the data acquisition with a sampling frequency of 1 kHz.

2.The dual FBG sensor are used with different bragg wavelengths. One sensor is designed to respond to the strain variations while other is designed more sensitive to the temperature variation. The temperature dual FBG sensor is encapsulated inside a stainless-steel tube.

3.Additional temperature sensor T107 temperature probe is used to compare the temperature measurement with the calibrated stainless-steel tube encapsulated FBG sensors. We have also monitored the room temperature using another thermocouple.
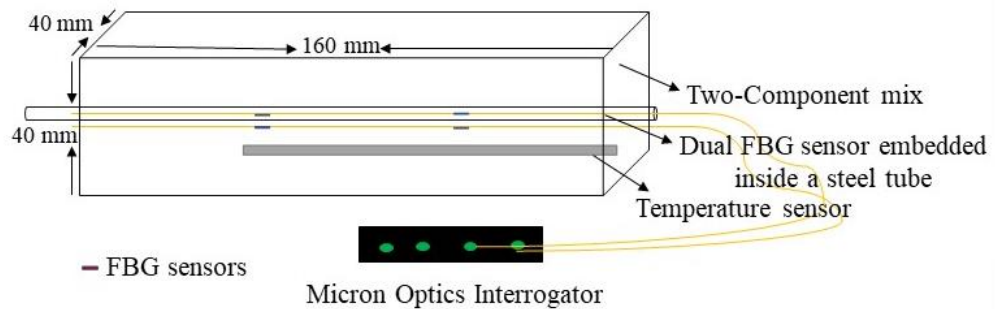
Figure 3. 2 : Schematic diagram of experimental setup.

The casting of the four mix designs are done according to (Todaro and Pace 2022b)and the shape of the casting mould is 40mm*40mm*160mm.As shown in *Figure 3. 2* before casting the dual FBG sensors, steel tube encapsulated the dual FBG sensor, and the temperature sensor (T107-temperature probe) was inserted into the casting mould of dimension (40 mm* 40 mm* 160mm) horizontally through the centre and parallel to the casting mould. The Bragg wavelength of the dual FBG sensors is summarized in *Table 3. 4* The bare FBG sensor is placed directly in contact with the mix and the temperature FBG sensor is isolated from contacting the mix by encapsulating inside a stainless-steel tube. T107 sensor is a temperature probe used for measuring the temperature of air, water, and soil. It consists of a thermoresistor, encapsulated in an epoxy-filled aluminium housing. This probe is used to compare the temperature measurements from the FBG temperature sensor. These FBG sensors are spliced to the optical patch cord and connected to the micron optics interrogator.

Table 3. 4 : Bragg wavelength of the FBG sensor for different Bentonite.

Bentonites	Bare FBG sensor		Temperature FBG sensor	
	A	B	A	B
B1	1537.924 nm	1545.778 nm	1545.768 nm	1537.876 nm
B2	1537.874 nm	1545.769 nm	1545.779 nm	1537.923 nm
B3	1546.011 nm	1537.893 nm	1538.268 nm	1546.190 nm
B4	1529.808 nm	1537.936 nm	1537.910 nm	1529.837 nm
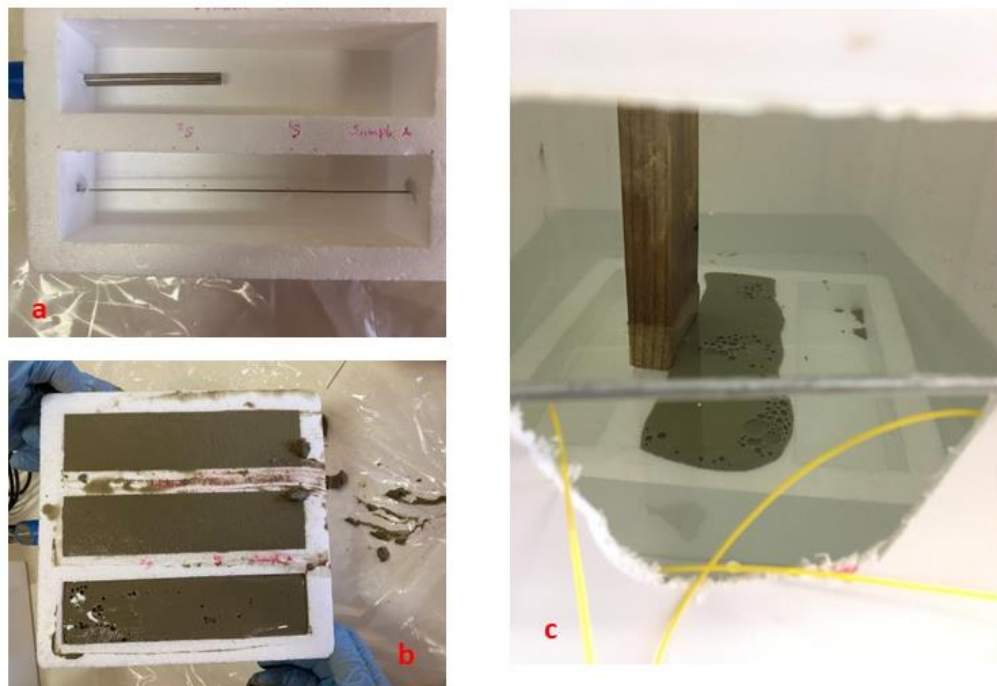
Figure 3. 3 : Preparation of FBG sensor in the casting moulds (a) Before casting, (b) After casting, (c) place the moulds inside the water bath after casting.

The mix designs are prepared based on the proportion given in *Table 3. 1*and *Table 3. 2*. When the mix design is ready, they are poured into the casting moulds

as shown in *Figure 3. 3*(a). This mixing should be executed rapidly to achieve a uniform grout flow into the mould. Once the mould is filled after 30 to 60 seconds, the sample's surface is scraped using a spatula to obtain a flat surface as depicted in *Figure 3. 3*(b). Then these samples are kept in a water bath *Figure 3. 3*(c) for the rest of the days during the measurement of shrinkage and temperature.

Another test was done to see the influence of keeping the sample inside the water bath for the B1 mix design by keeping them 5 days outside in room temperature.

3.3 Results

3.3.1 Temperature Calibration

The parameters than can affect the shift in the wavelength is thickness and thermal conductivity of the encapsulated tubes. From Figure (3.4) it can be noticed that the stainless-steel encapsulated material provides more shift in bragg wavelength compared to the borosilicate glass with same thickness can be due to the thermal conductivity of stainless steel is more than the borosilicate glass. The sensor encapsulated inside the stainless-steel tube is used for the measurement of early age temperature change. The estimated thermal sensitivity of stainless steel encapsulated dual FBG sensor is 11.8 pm/ ^{0}C.
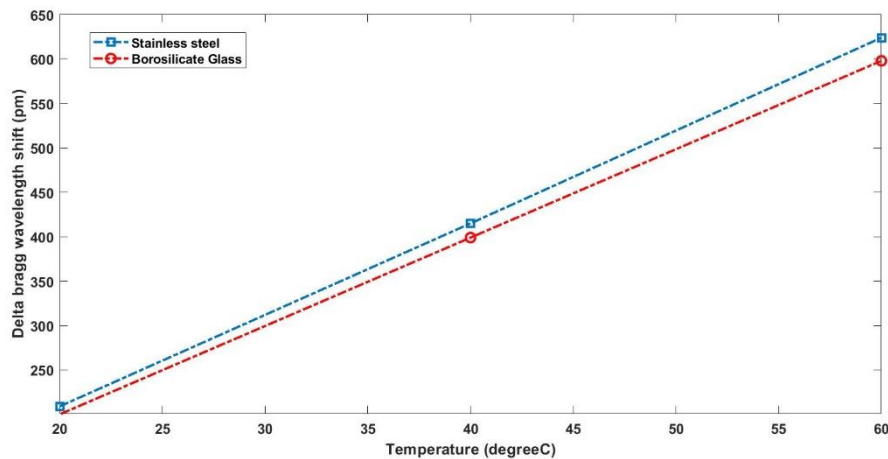
Figure 3. 4 : Temperature response of encapsulated FBG from 20 ^{0}C – 60 ^{0}C

3.3.2 Shrinkage and Temperature of Mix Designs

3.3.3.1 Temperature measurement

The temperature change of the mix design in the first 16 days after the casting is shown in *Figure 3. 5*and *Figure 3. 6*.It is observed from the plots the temperature measurement of the two-component mix with bentonite B1 with the temperature probe T107 and the measurement from the encapsulated FBG sensor is the same. We observe the temperature kept increasing in the initial hours with a slowing down. This increase can be due to the expansion of the mix by the absorption of water during the hydration of cement. As hydration is an exothermic reaction happening during the setting, which releases heat and results in the temperature rise. So, we observe a sharp increase in the temperature. In the mix design with bentonite B1 we observe a temperature change of 2 degrees.
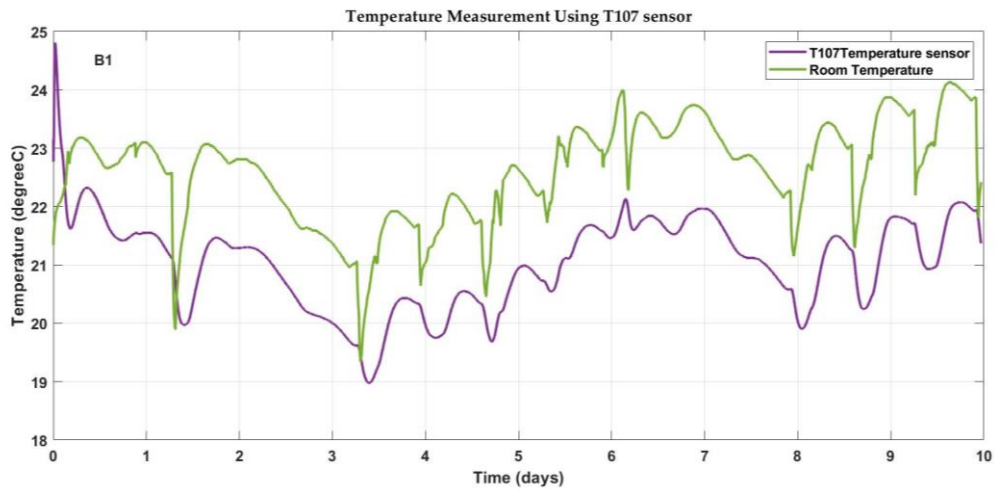
Figure 3. 5 : Temperature Measurement of B1 with T107 sensor and the room temperature.
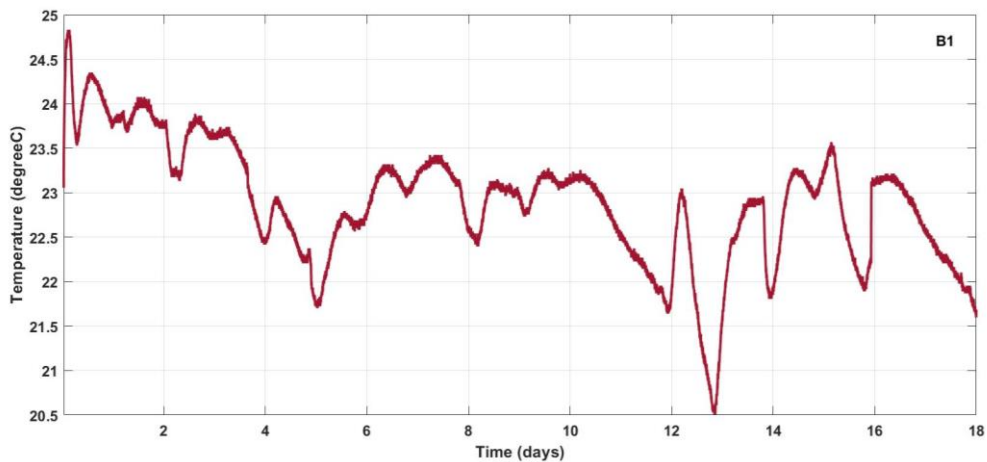
Figure 3. 6 : Temperature Measurement of the mix using FBG sensor.

Figure 3. 7 shown below is the temperature measurement of the mix design with bentonite B1, B2, B3, and B4 in the 24 hours after casting. As from the previous plot, it is observed the temperature change occurs in the initial hours of setting. The temperature change for all these mix designs is increased by almost 4 degrees from the start. The peak temperature is at about 90 minutes and then dropped at about 360 minutes (6 hours). From the temperature measurements, the final setting time of the mix is when the temperature is reached maximum and that is about 90 minutes after casting.
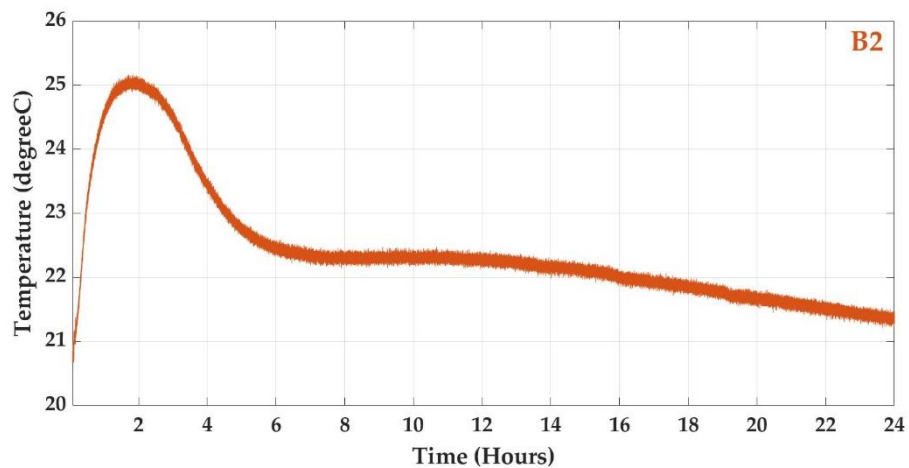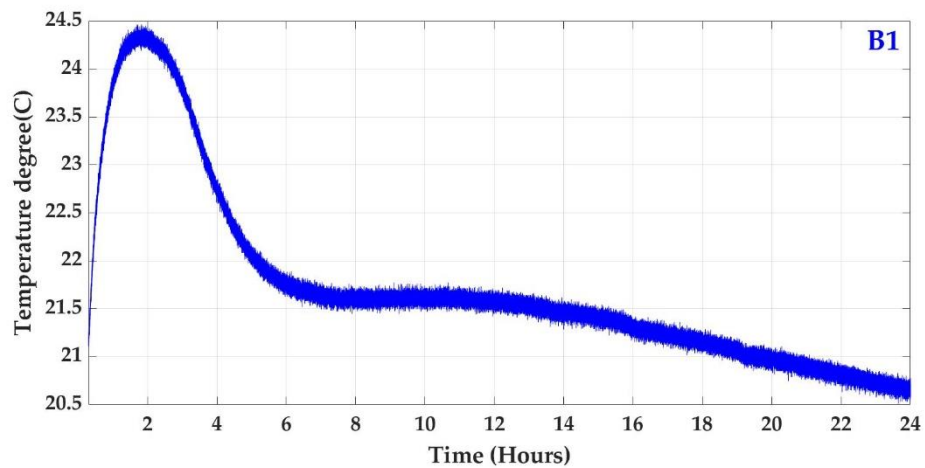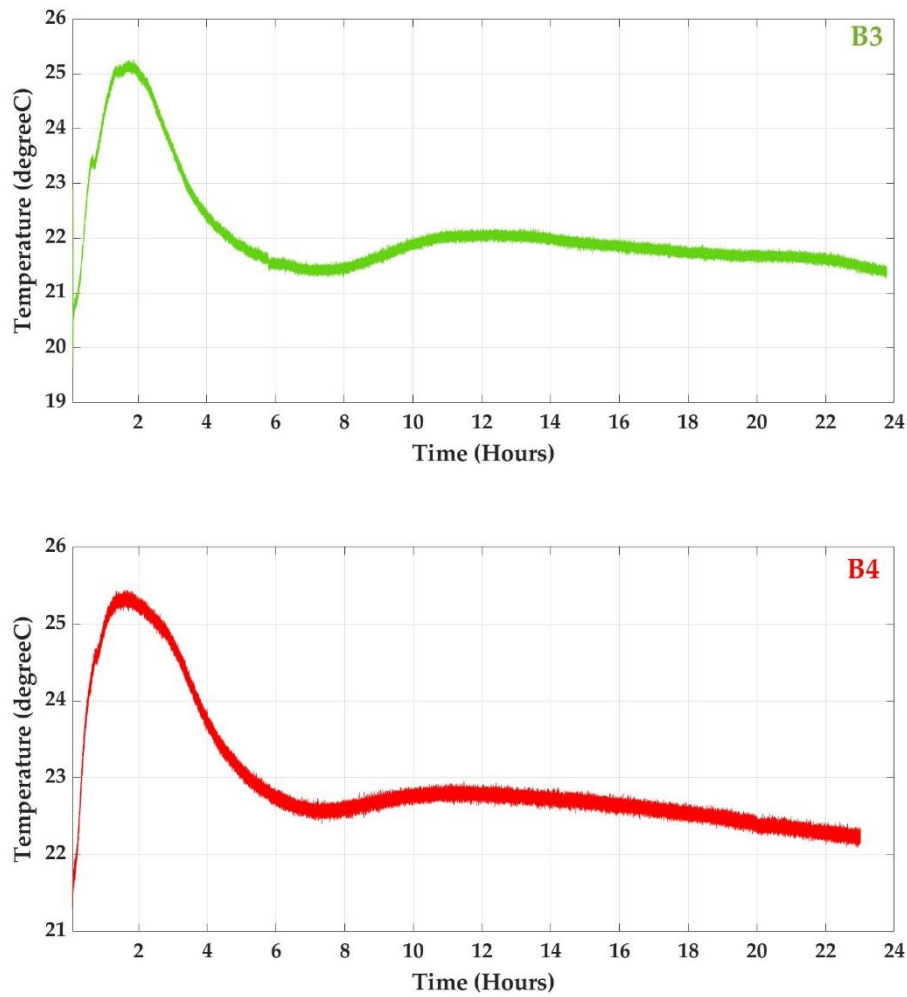
Figure 3. 7: Temperature Measurement of B1, B2, B3 and B4 using FBG sensor.

3.3.3.2 Shrinkage measurement up to 16 days

The shrinkage measurement is done for 16 days after the casting. The shrinkage plot of the bentonites is shown in *Figure 3. 8*. It is observed from the plots the early age shrinkage of bentonite B1 is more than the other bentonites and 50 percent of the shrinkage happens in the initial hours of casting then it is decreased gradually and remains at a constant value at about 16 days of casting. This prolonged shrinkage in the initial phase is because of temperature due to hydration.
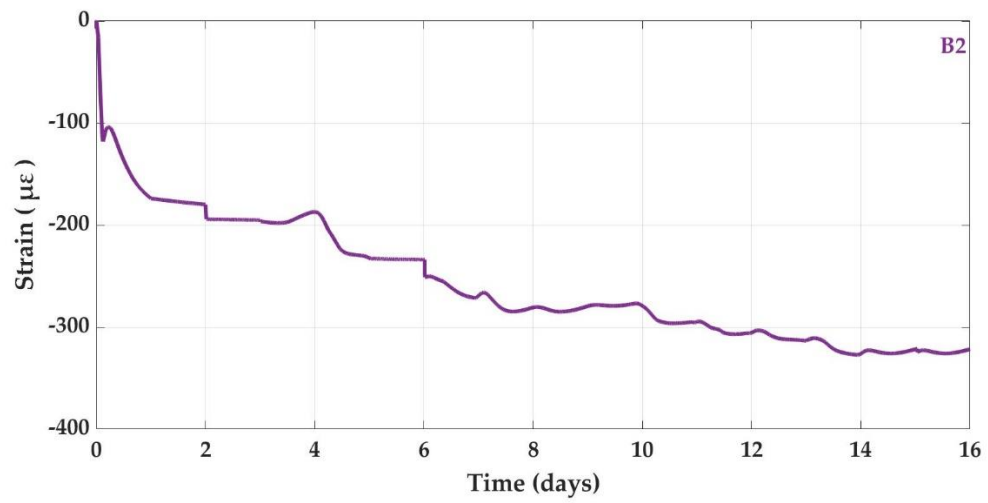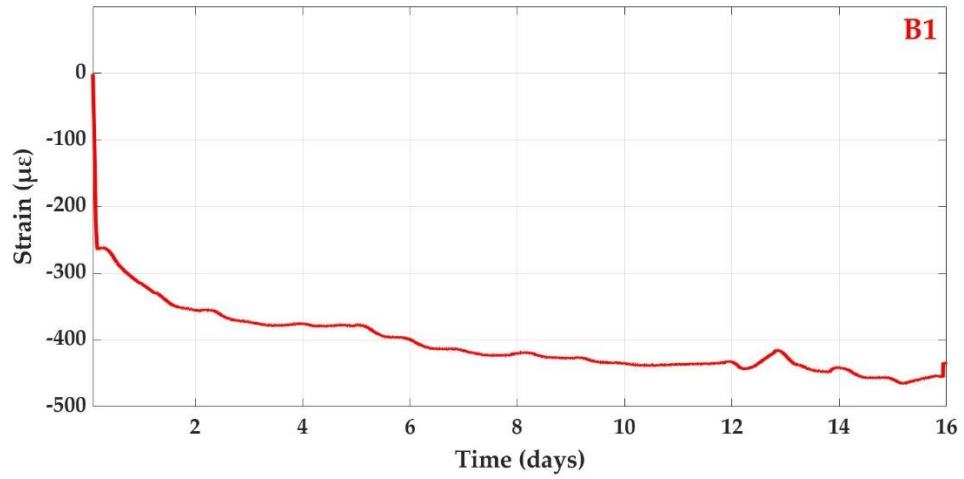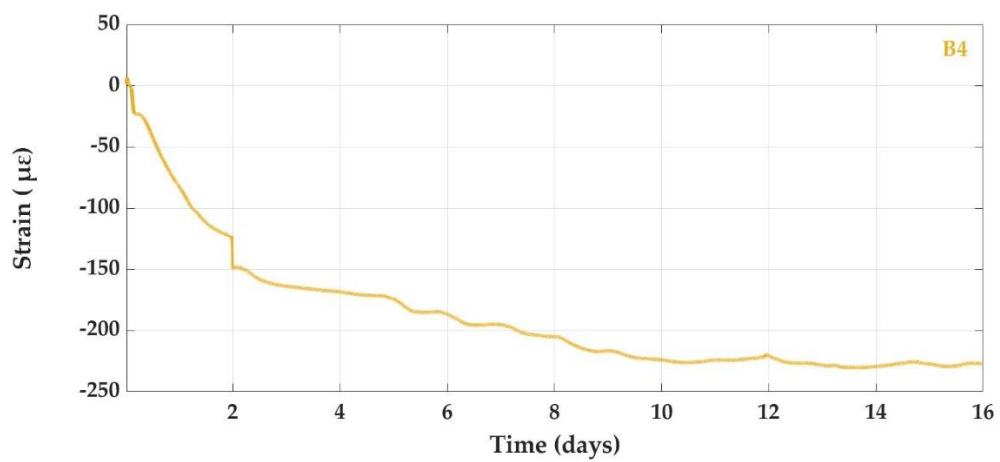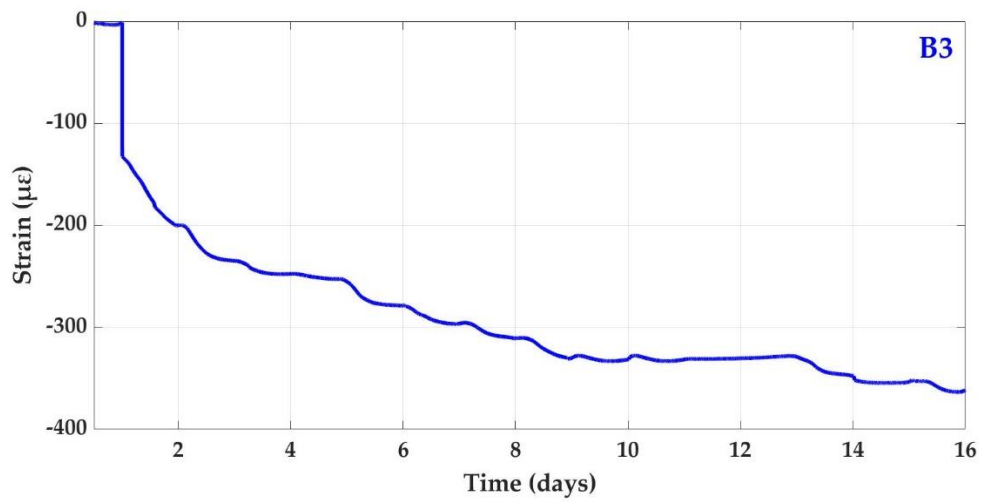
Figure 3. 8 : Early age shrinkage of different bentonites B1, B2,B3 and B4.
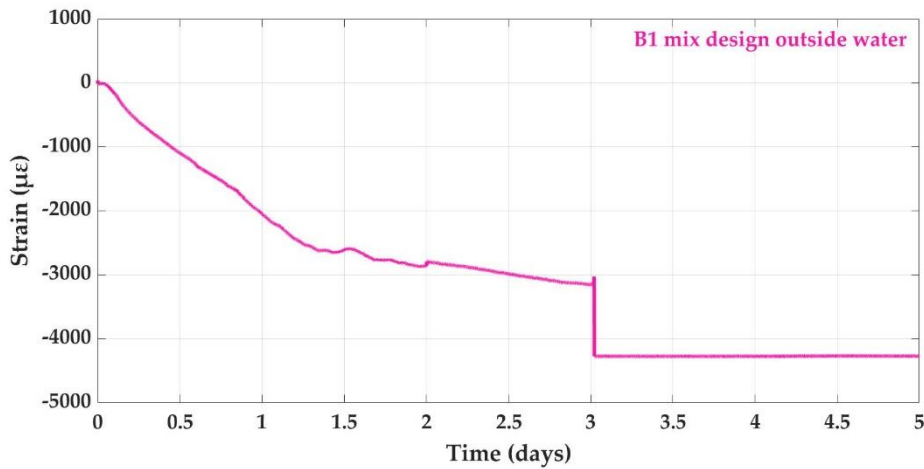
Figure 3. 9 : Early age shrinkage of B1 bentonite mix design kept outside the water bath.

From *Figure 3. 9*, it can be noticed from the excessive shrinkage that sample losses the natural water and there by the mechanical properties when kept outside.

3.4 Discussion

From the early age temperature analysis, the temperature kept increasing in the initial hours with a slowing down. This increase could be due to the expansion of the mix by the absorption of water during the hydration of cement. As hydration is an exothermic reaction happening during the setting, which releases heat and results in a sharp increase in the temperature. The peak temperature is at about 90 minutes and then drops at about 360 minutes (6 hours). From the temperature measurements, the final setting time of the mix is when the temperature is reached maximum and that is about 90 minutes after casting. This stage defines the setting stage of the two-component mix. The temperature change is very less from 2 degrees to 4 degrees for different mix designs. This trend is similar for all mixes, irrespective of the used bentonite.

The early age shrinkage measurement is done 16 days from the casting. It is observed from the plots the early age shrinkage of bentonite B1 is more than the other bentonites and 50 % of the shrinkage happens in the initial hours of casting then it decreases gradually and remains at a constant value at about 16 days of casting. The maximum shrinkage is for the mix B1 (about 450 µɛ) while the minimum shrinkage is for the mix B4 (about 250 µɛ). The difference in values of shrinkage can be due to the different used bentonite. However, it is not possible to correlate the differences found with the bentonite index considered in this research

(SWI and smectite content). The difficulty in correlating the behaviour of a certain two-component grout and the used bentonite is confirmed also in the scientific literature (Todaro and Pace, 2022; Todaro et al., 2023). Analysis of the shrinkage by keeping the mix design outside the water also concludes that its losses of the natural water and mechanical properties are the reason for the excessive shrinkage.

The analysis of the shrinkage put alight the very limited magnitude of the phenomenon (< 500 µε), abundantly within the threshold value of 10000 µε reported in the technical specification of some tunnel construction sites (Càmara, 2018; Todaro et al., 2022a).

From this analysis, we can conclude that all the tested mix-design are suitable for backfilling in the tunnel.

3.5 Conclusions

We investigated the early age shrinkage and temperature of the two-component grout. Fiber Bragg Grating technology has been successfully employed for the early age analysis. The ability of FBG to multiplex, non-destructive and immune to EMI is an added advantage of the measurement compared with the conventional sensor.

Since the bragg wavelength shift is affected by both the strain and thermal changes in the grating region, hence distinguishing and isolating the response is necessary when simultaneously measuring the shrinkage and temperature. This discrimination of strain and temperature is achieved by using two dual FBG sensors with one of the dual FBG being free and the other dual FBG being packaged inside an encapsulated tube in an identical situation. After the calibration of the sensors encapsulated in the borosilicate glass and stainless-steel tube. We observed the encapsulation was better in the stainless-steel tube.

Thus, FBG sensors have proven useful for investigating the early age properties of two component mix. One of the limitations of this technique is the fragility of the sensors and the installation of them should be taken care. We still have room for improving the packaging of the FBG temperature sensors and developing the FBG strain sensor instead of the bare sensor for the strain measurement to make the system more rigid and robust, for further studying about this component with different water to cement ratio and by changing other properties.

Chapter

Dynamic Monitoring

4.1 Introduction

Recently, there has been a tremendous improvement in seismic networks in terms of instrumentation, and technologies providing high-resolution data (Z. Li 2021). Generally, based on the field of application seismic acquisitions require instrumentation with different sensitivity and frequency ranges. Earthquake signals oscillate in a frequency range of 0.1-1 Hz; recording these signals requires high-sensitivity and low-frequency range sensors. In civil engineering, higher frequency is usually required for structural health monitoring of bridges and buildings. This instrumentation is characterized by low resonant frequency to measure the low-frequency signals generated by mechanical, active seismic sources and the sensor should record a large bandwidth to avoid the loss of frequency components in the recorded signal and simultaneously record different seismic sources.

Existing accelerometers can be categorized into electronic and optical accelerometers. Electronic accelerometers like micro-electromechanical (MEMS)(Scudero et al. 2018), piezo resistive, capacitive, piezoelectric, and resistive sensors are commonly used (Elies 2015). The electro-mechanical accelerometers mainly consist of a mass attached to the reference frame. The working principle is based on the deflection of the proof mass due to the acceleration applied to the reference frame. Piezoelectric accelerometers are instead based on the piezoelectric response of some specific material, and they have advantages like low cost, ease to handle and implementation due to their solid construction, wide frequency range, and temperature stability. On the other hand, they exhibit criticality because of low linearity and under constant force there is leakage in the charge generated on the piezoelectric element hence do not have the DC response. Piezoresistive accelerometers are suitable for low frequency, small volume, low linearity, and measure static as well as dynamic acceleration (DC response) but could be sensitive to temperature. Capacitive accelerometers are low cost, low power consumption, high sensitivity, DC response but are interfered with

the external environment and suitable for low-frequency fields. All these systems are vulnerable to electromagnetic interference because of their sensing principle (Sotnik and Lyashenko 2022).

The optical accelerometers are mainly based on fiber optic sensing technology. Fiber optic sensing techniques like Distributed Acoustic Sensing (DAS) (Z. Li 2021; Z. He and Liu 2021; Ashry et al. 2022; Lindsey and Martin 2021), Fiber Bragg Grating (FBG) (Baldwin et al. 2005; Y. Guo et al. 2021; T. Li et al. 2020), and Fiber Fabry Perot Interferometer (FFPI) (Gangopadhyay 2004; García, Corres, and Goicoechea 2010; Rao, Ran, and Gong 2017; C. Zhu et al. 2023) have been extensively studied for vibration measurements in recent decades. Compared to the other accelerometers they are immune to electromagnetic interference. They also show high sensitivity, compactness, capability to transmit signals at long distance, DC response, wide bandwidth, corrosion resistance, high temperature and pressure resistance. Competing with other optical accelerometers, Fiber Bragg Grating-based sensors have undergone rapid development and established as the leading technology for onsite measurements in structural monitoring, for vibrational acceleration measurement of low-medium frequency ranges with high sensitivity.

Various cantilever beam-type accelerometers of Fiber Bragg Grating have been reported in the past decades. (Wu et al. 2009) analysed the potentialities of three different FBG-based accelerometers for the study of different seismic measurements. Later, Hz (da Costa Antunes et al. 2009) proposed a L-shaped cantilever beam accelerometer suitable to monitor frequency up to 45. A compact FBG diaphragm accelerometer with L-shaped and U-shaped rigid cantilever beam, with wide frequency range and high sensitivity, was reported by (Weng et al. 2012; Yinyan Weng et al. 2011).An alternative approach was developed by (N. Basumallick et al. 2012; Nandini Basumallick et al. 2013) to enhance the sensitivity (450 pm/g) by increasing the distance between the neutral axis of the fiber and the axis of fiber using a backing patch. (Dingyi Feng et al. 2015) demonstrated a hybridized two cantilever FBG accelerometer with temperature compensation and minimum cross axis sensitivity. (Casas-Ramos et al. 2017; Casas-Ramos et al. 2018; Miguel Angel Casas-Ramos et al. 2015) put forward a sensor design by improving the resonant frequency without affecting the sensitivity. Guo et al. (2020) suggested the fabrication of vibrating element in the FBG accelerometer with 3D printing Technology. (Zhang et al. 2014) proposed a double semi-circle cantilever beam with high sensitivity and minimum detectable frequency of 5 Hz.(Hong et al. 2021) designed a multi-cantilever beam mainly composed of three rectangular cantilever beams with low frequency, within the range of 16-54 Hz and

a sensitivity of 87.955 pm/g.(Hafizi and Vorathin 2021a) proposed a low-frequency FBG accelerometer based on a Polyphenylene Ether (PPE) thermoplastic cantilever beam with a sensitivity of 110 pm/g and a natural frequency of 9 Hz.

However, the reported literature studies on FBG accelerometers are mainly concentrated on the design, fabrication, and experiments in the lab. There remains a need for the efficient study of the reliability of these systems in terms of packaging, installation for practical applications, especially in real field cases.

Aiming at the problem of reliability of these systems in the practical applications, we design, optimize, and test this traditional cantilever beam-based accelerometer in the field in comparison with the standard geophones; the main goal was to check the suitability of the proposed sensors for picking up the first arrival time (travel times), that is a common value estimated in seismic exploration. This accelerometer was theoretically and experimentally analysed in terms of sensitivity and natural frequency; moreover, the theoretical simulations and design optimizations were undertaken with the ANSYS software. The proposed design is fabricated with the help of 3D printing technology and packaged in a cost-effective way. Experimental results from the laboratory shows that the sensor has a flat frequency response from 5 to 55 Hz. The sensitivity of the accelerometer is ±433.7 pm/g with natural frequency of 75 Hz. The preliminarily test performed in the field in comparison with common electro-mechanical geophones for picking up the first arrival time was successful for verifying its effectiveness in seismic vibration measurements.

4.2 Methodology

4.2.1 System Description

Fiber Bragg Gratings (FBGs) are formed by the periodic modulation of the refractive index along the longitudinal direction of the photosensitive single-mode fiber core (Hill and Meltz 1997). The peak wavelength reflected by the FBG is the Bragg reflection wavelength and is mainly dependent on the effective refractive index of the fiber core and the period of the grating. Any change in the effective refractive index or the grating period will cause a shift in the Bragg wavelength. This shift can be used to measure various physical parameters, like temperature, strain, etc. Typical value of strain and temperature sensitivity of standard FBG sensors are 1.2 pm/$\mu\varepsilon$ (micro strain) and 13 pm/°C respectively (Campanella et al. 2018). These FBG sensors are sensitive to both strain and temperature variations

directly but can indirectly be exploited to quantify other physical parameters, like pressure, displacement, and vibration by using transducers, e.g., specifically designed elastic structures, to relate them to axial strain (Y. Guo et al. 2021).

We propose a FBG cantilever beam-based accelerometer that could be customized to adjust sensitivity and resonant frequency. The mechanical structure of the accelerometer is a single cantilever beam with mass block at its tip suspended at a certain height within an encasing structure. FBG is positioned and fixed perpendicular to the surface of the vibrating cantilever beam through a hole made in the encasing structure. The schematic diagram of the proposed cantilever mass-based accelerometer is presented in the (*Figure 4. 1*). Here FBG is used as a spring that enhances the natural frequency of the cantilever and uniformly strains the grating to increase the sensitivity of the system to vibrations. Pretension is applied for the FBG by gluing in two points at the end of the cantilever beam and the encasing structure with a white epoxy adhesive. This epoxy is mainly used in structural bonding applications for high chemical and temperature resistance. The interference of the epoxy on the FBG sensor is not considered in this study.
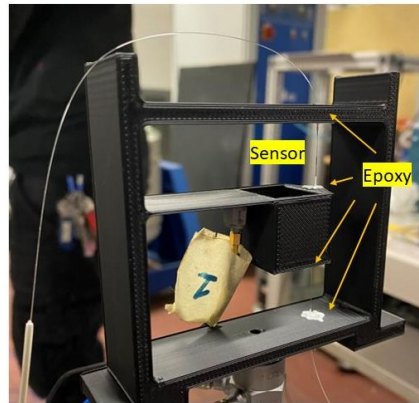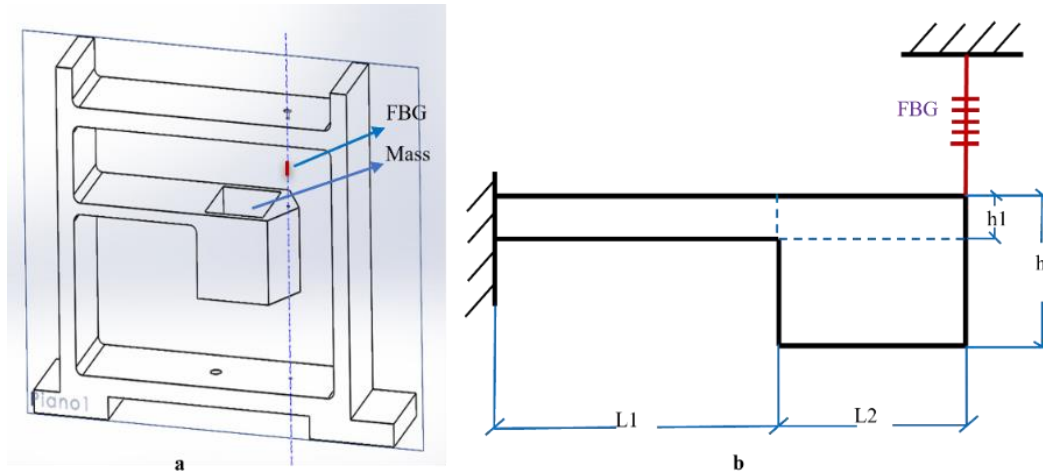
Figure 4. 1 : Structure of the cantilever beam based FBG sensor: (a) system 3D rendering generated by Solid Works (2020); (b) schematic section of the cantilever;(c)close shot picture of sensor, epoxy attachment area.

When a vibration is applied at the base of the structure, the acceleration induces a force on the mass block resulting in the deflection of the cantilever beam. The vertical deflection of the cantilever beam elongates the gratings of FBG resulting in the Bragg wavelength shifts due to strain. This corresponding bending strain is proportional to the vertical acceleration. Hence this system is more sensitive to the vertical axis. The response and resonance along the other two components are consequently not taken into consideration in this study.

The natural frequency and the sensitivity of the proposed design is increased by placing the FBG sensor at the maximum bending point, which uniformly strains the FBG axially with the vertical axis. The sensitivity, operational bandwidth and natural frequency of the proposed design can be tailored by changing the

cantilever beam parameters (length, breadth, and thickness), weight of mass block, material of the cantilever beam and mass block which depends on the young's modulus and density of the material.

4.2.2 Preliminary Test

A preliminary lab test was carried out on an FBG sensor having the same design described in (Cavalli 2018), having a (theoretical) resonance frequency of 128 Hz and sensitivity of 956 pm/g. The sensor structure consists of a cantilever beam with a Cantilever length (L1) of 30 mm, a mass block length (L2) of 20 mm, total length of cantilever beam (L=L1+L2) of 50 mm, breadth of 20 mm, thickness (h1) of 5 mm (*Figure 4. 1* (b)); a block mass of lead (88 g) is inserted at the tip of the cantilever beam. The whole system is fabricated with polylactic acid (PLA) by 3D printing. The elastic modulus and the cross section of the fiber optic SMF-28 with protective coating is considered from (Paulo Antunes et al. 2012; P. Antunes et al. 2008). The FBG used in this system has a central wavelength of 1538.12 nm, reflectivity≥90%, and length of 10 mm. This sensor was spliced to the fiber patch cord and connected to the SMART SCAN Interrogator for data acquisition with a sampling frequency of 500 Hz. This is a Wavelength Division Multiplexing instrument with a tunable laser source that enables high resolution at multi-kHz frequencies and consists of four optical channels hence multiple sensors can be multiplexed without reducing the speed and performance.

We compared this FBG cantilever system with a common 4.5-Hz vertical geophone used for active seismic recording (*Figure 4. 2*), connected to a Geode Exploration Seismograph (Geometrics). A light hammer was used to generate vibrations to be recorded by both instruments. The geophone system was automatically triggered (time =0 s corresponds to the impact of the hammer), while the recording of the FBG system was manually triggered by the operator during the test.
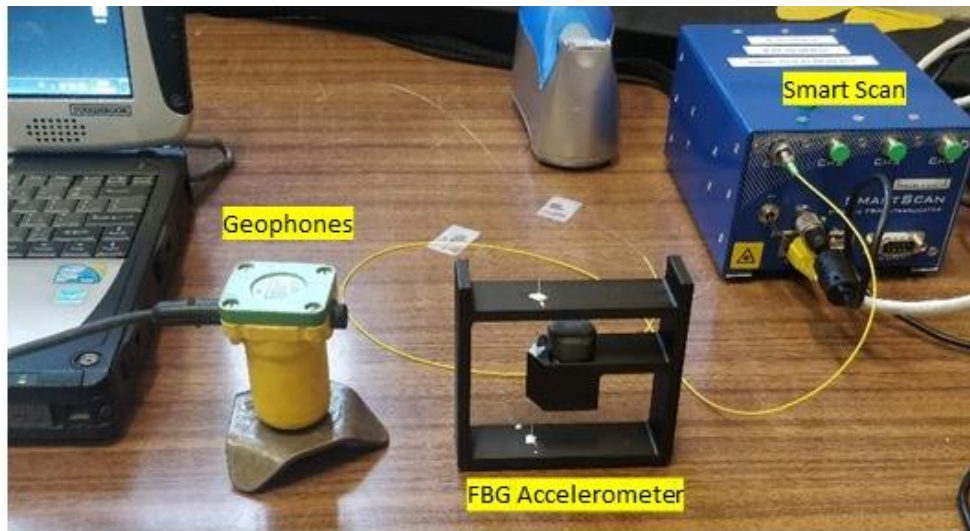
Figure 4. 2 : Comparison test between the FBG accelerometer and a standard vertical 4.5 Hz geophone in the laboratory with external hammer shots.

Data recorded from both systems were analysed with on-purpose compiled MATLAB codes, to compare their time- and frequency-domain content. In (*Figure 4. 3*)exemplificative signals (*Figure 4. 3 a,d*), related normalized amplitude spectra (*Figure **4. 3** b,e*) and spectrograms (*Figure 4. 3 c,f*) are shown for the FBG accelerometer and the standard geophone respectively.A time shift can be noticed between the first signal recorded by the two systems as a consequence of the lacking triggering system for the FBG sensors. Nevertheless, the time delay of the following signals with respect to the first one is the same for both the systems.
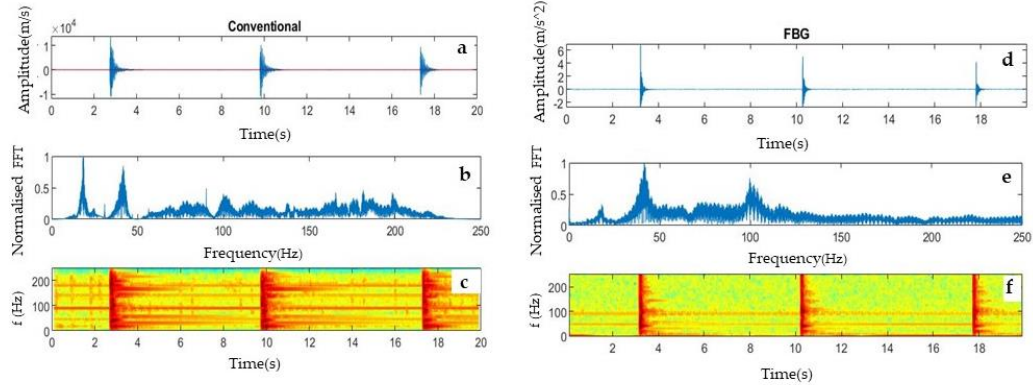
Figure 4. 3 : Exemplificative comparison of time- and frequency- domain signals from the conventional geophone (left) and the FBG system (right) in the preliminary laboratory test. (a) Amplitude of the signal of the conventional geophone in the time domain, (b) normalized amplitude spectrum, (c) spectrogram,(d) amplitude of the signal of FBG accelerometer in the time domain, (e) normalized amplitude spectrum , (f) spectrogram.

The results from the preliminary test showed promising potential for recording seismic vibrations. Nevertheless, the FBG sensor recordings showed lacking information related to the first signal onset. Using the spectral amplitude of the geophone as a reference, the FBG sensor showed lower sensitivity in the low-frequency range, below 20 Hz. Similar spectral peaks are detected by both instruments, but with different amplitudes. These preliminary results highlighted the need for numerical optimization of the system configuration for improving the sensitivity of the system in the low frequency range. The accelerometer design was further optimized by theoretical simulations using ANSYS finite element modelling software are reported in Section 4.2.3.

4.2.3 Numerical simulations of the effect of structural parameters on the natural frequency

The length, breadth, and height of the cantilever beam are the key parameters affecting the sensor sensitivity S and natural frequency F_0. The natural frequency of the sensor is mainly ruling on the possible measuring range and the vibration

performance of the sensor. To study the effect of the system geometry on the natural frequency, cantilever beams with various dimensions were modelled and their response was simulated with the finite element modelling software ANSYS Student (2023).

Modal analysis is an analytical method for determining the vibration characteristics of the design. In this analysis, we obtain the natural frequencies and modes of the different sensor designs. Here, the modal analysis of the design was conducted to calculate, solve, and extract the natural frequency of the first six vibration modes. The system structure was 3D printed with PLA, so the material properties adopted in the simulation was easily user defined with the parameters summarized in (*Table 4. 1*). The block mass (20 g) inserted at the tip of the cantilever is made of lead.

Table 4. 1 : Material Properties adopted in the simulations.

Physical and Mechanical Parameters	*PLA*	*Lead*
Young's Modulus (Pa)	4.1E7	5.5E6
Density (kg/m³)	1290	9670
Poisson's Ratio (-)	0.3	0.4

During the simulations, the base of the system (*Figure 4. 1* (a)) was set as a fixed constraint to consider the coupling with the ground surface. The remaining domains and boundaries were left free to vibrate. The displacement of the beam was set free in the y direction and constant in the other two directions.

In the simulation, we have considered cantilever lengths (L1 in *Figure 4. 1* (b)) within the range of 30-45 mm at three different heights (1 mm, 3 mm, and 5 mm, h1 in *Figure 4. 1* (b)) by keeping the cantilever's breadth constant (20 mm). A total of twelve configurations were consequently simulated and analysed for the estimation of the natural frequency of the system.
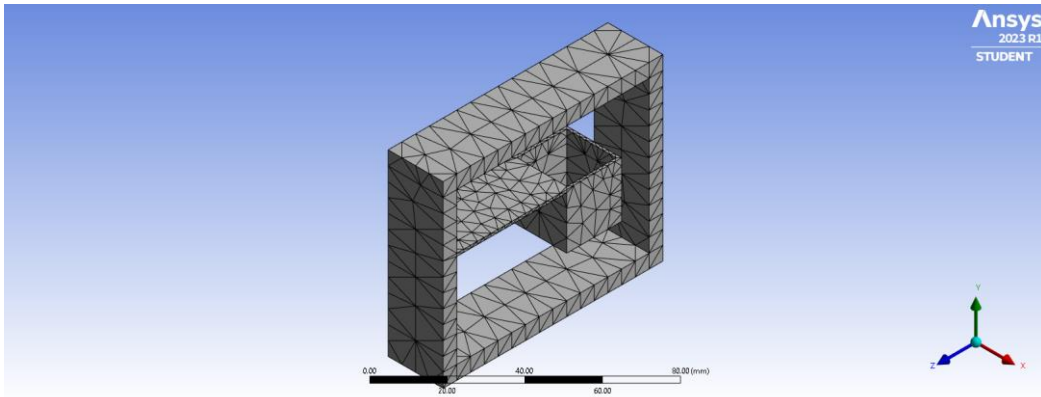
Figure 4. 4 Mesh of the Cantilever based FBG accelerometer.

After the numerical simulation these selected configurations are 3D printed using PLA. The structure is printed in a layered manner as shown in the *Figure 4. 5* The 3D printer used here has high repeatability of about (X/Y) +/- 0.1 mm. We measured the geometry from the CAD model and the 3D printed sensor with the help of a vernier caliper and based on macro-scale observation percentage deviation was very less hence the metrological performance was not affected by peel-off and sintering. From the literature review, PLA material is used for the development of sensors which has a typical shrinkage of about 2%. And again, since this work is concentrated on the development of sensors for monitoring active seismic sources by picking up the first arrival time, not on the manufacturing.
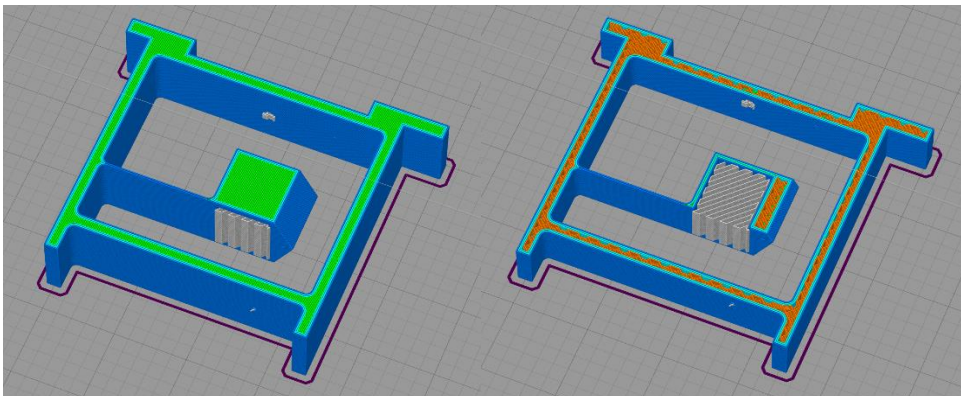
Figure 4. 5 : 3D printing of the structure in a layered manner.

4.2.4 Lab Calibration of the system

After numerical simulations, four system configurations were selected for laboratory calibration as summarized in (*Table 4. 2*). *Figure 4. 6* shows the schematic diagram of the vibrational shaker set up with the prototype FBG accelerometer and vibration exciter. The amplitude frequency response test is conducted by attaching the base of the FBG accelerometer to the Tira Vibrational shaker using glue. The vibrational shaker provides a linear oscillatory motion in the vertical direction. This device is paired with a Function generator and an amplifier. The input source of the vibrational shaker is a sweep signal (harmonic sinusoidal) with a sweep frequency ranging from 5 Hz to 110 Hz at a peak acceleration of 0.1 g at intervals of 5 Hz with a time lag of 10 s at each frequency. Near to the simulated resonance frequency the outputs are recorded at a smaller interval of 1 Hz for tracking the exact natural frequency. A Micron Optics Si155 interrogator system was used to acquire the data of FBG wavelength shift with a sampling frequency of 1 kHz. This system can potentially acquire the measurements of hundreds of sensors on four parallel and 160 nm wide optical channels.

Table 4. 2 : Configuration of the systems used for Lab Calibration.

	Cantilever Length (mm)	*Cantilever Thickness (mm)*
1	30	1
2	30	3
3	40	1
4	40	3
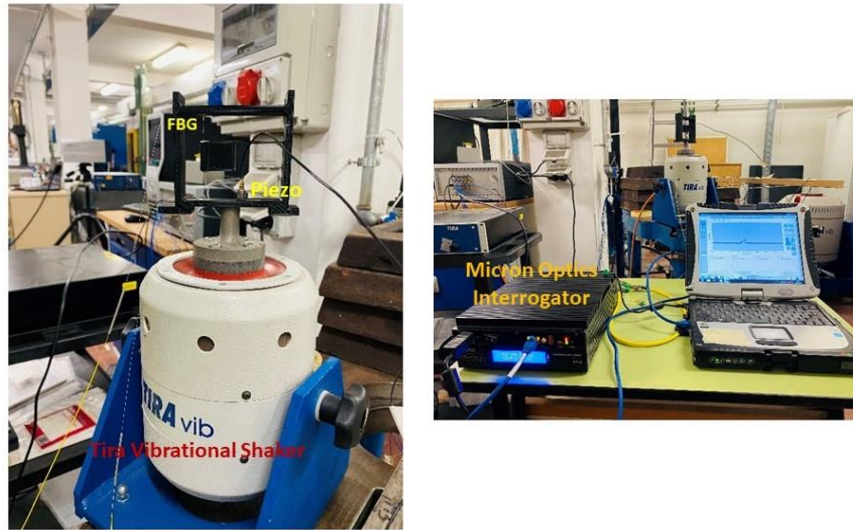
Figure 4. 6 : Laboratory Calibration of FBG system with a mechanical shaker.

The dynamic sensitivity at different frequencies was tested by varying the Vpp (peak to peak voltage) from 0.2 to 1 with the step size of 0.2, with frequency of the vibration of the shaker set to 20 Hz. We repeated the same experiment at frequencies of 10, 30 and 40 Hz. A piezo-electric accelerometer with a frequency response from 0 to 20 kHz was additionally placed on the base of the system, as a reference measure without altering the cantilever response. The sensitivity was calculated by dividing the wavelength shift from the data measured by Micron Optics Interrogator by the corresponding acceleration observed by the piezo accelerometer.

4.3 Results

The primary mode of vibration from the ANSYS Modal analysis is shown in (*Figure 4. 7*)for one of the simulated configurations (L1=40 mm, thickness 1 mm and width 20 mm). The resonance frequencies of the first six orders are reported in for the same system configuration.
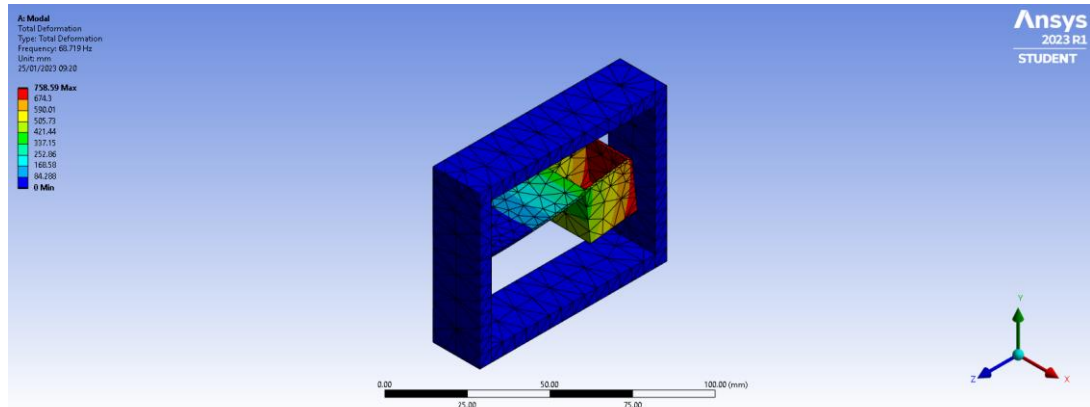
Figure 4. 7 :First vibration mode in Modal Analysis for system configuration having cantilever length of 40 mm, thickness of 1 mm and breadth of 20 mm.

Table 4. 3 : First six resonance frequencies (Hz) obtained for the system configuration of Figure 4. 6

Order	First	Second	Third	Fourth	Fifth	Sixth
Resonance Frequency (Hz)	68.7	212.8	415.8	684.2	941.9	1271.0

As shown in *Figure 4. 8*, the simulated natural frequency of the system decreases with the increase in the cantilever beam length from 30 mm to 45 mm. In systems having the same cantilever beam length, the natural frequency increases and with the increase in the cantilever beam thickness.
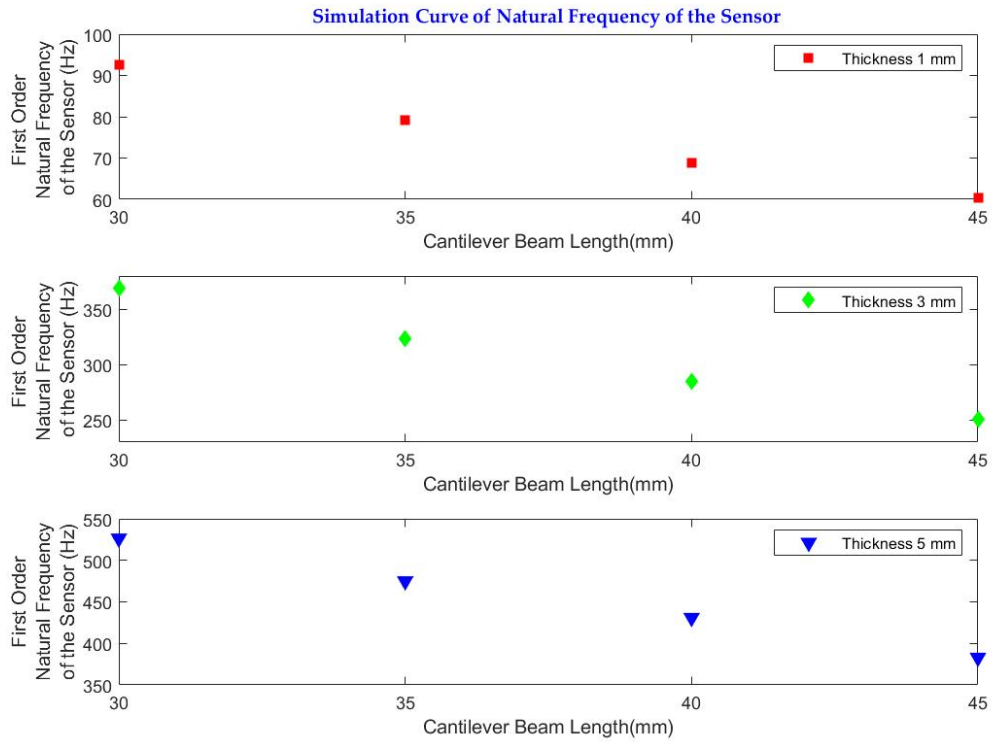
Figure 4. 8 : Sensitivity analysis of natural frequency values for different cantilever beam lengths and thicknesses.

Based on the results of the sensitivity analysis, the cantilever configuration having the lower natural frequency (68.7 Hz) was selected to be printed and further tested in the lab and field experiments. The geometry and structure of the selected configuration are summarized in *Table 4. 4*

Table 4. 4 : Cantilever beam configuration for laboratory and field tests.

Parameter	Value
Length of cantilever (L1)	40 mm
Mass Block length (L2)	20 mm

Total Length of Cantilever (L=L1+L2)	60 mm
Width of the cantilever beam	20 mm
Thickness of the cantilever beam	1 mm
Fiber length from enclosure to the cantilever tip	20 mm
Lead mass	20 g

For this system configuration, the amplitude frequency response of the accelerometer retrieved from the laboratory calibration on the vibrational exciter is 75 Hz *Figure 4. 9*. The accelerometer shows an almost flat response within the range of 5-55 Hz, so being applicable for the measurement of low-frequency signals. There is no physical reason behind the asymmetric response of the frequency. These kind of asymmetric response were reported in (Hafizi and Vorathin 2021b) for the low frequency cantilever accelerometer. The theoretically calculated natural frequency (68.7 Hz) for this system configuration is close to the measured one (75 Hz). Minor discrepancies can be due to the mechanical losses during the gluing of the sensor to the vibration exciter.
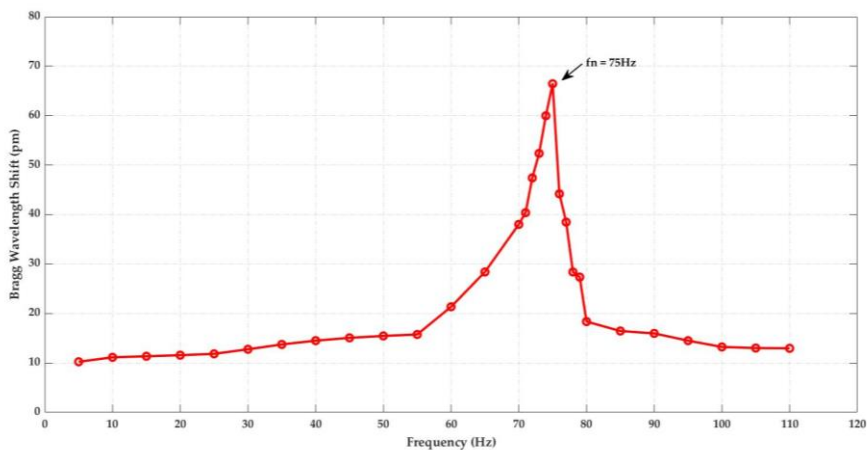
Figure 4. 9 : Amplitude -frequency response of the FBG accelerometer.

The dynamic sensitivity of the accelerometer was tested at the room temperature. The wavelength shift corresponding to different g values at 20 Hz are shown in *Figure 4. 10* as dots and the dashed line represent the linear fit. The slope of the linear fit gives the sensitivity of the sensor. The sensitivity of the sensor calculated from this experiment with fit coefficient R^2= 0.998 at 10 Hz, 20 Hz, 30 Hz and 40 Hz are ±435.1 pm/g, ±434.6 pm/g, ±409.3 pm/g and ±455.8 pm/g. The average sensitivity of this FBG accelerometer calculated from this experiment is ±433.7 pm/g with fit coefficient R^2= 0.998.
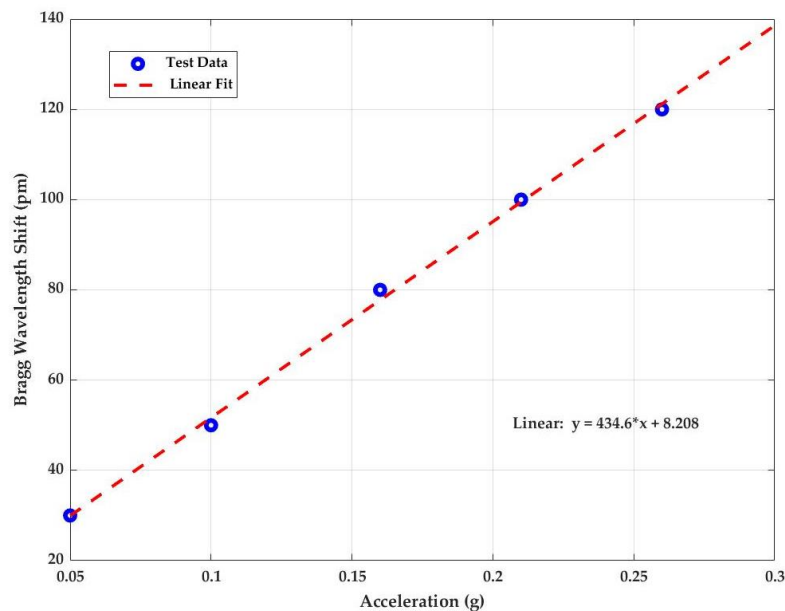
Figure 4. 10 : Linear response of Bragg wavelength shift versus applied acceleration at frequency 20 Hz.

4.4 Field Test of the Calibrated System

A preliminary field test was carried out with the calibrated FBG accelerometer from the FEM simulation and vibration exciter experiment. The final geometry has a length (L1+L2, in *Figure 4. 1*(a)) of 60 mm, a breadth of 20 mm, and a thickness (h1) of 1 mm. The cantilever is inserted in a structure with a size of 80 mm*65 mm and suspended at a high of 20 mm (*Figure 4. 1* (a)). The packaging of the system is

done by encasing the system inside a PVC box with two spikes attached at the bottom of the box to improve the coupling with the ground. Three FBG sensors with this configuration were used for the field test, with FBG length of 10 mm, central wavelengths of 1532.45 nm, 1538.65 nm, and 1546.12 nm, and reflectivity $\geq$ 90%.

The field test was conducted to compare the three serially connected packaged FBG accelerometers with five parallelly connected 4.5-Hz vertical geophones, as shown in *Figure 4. 11* and *Figure 4. 12* .The 4.5 Hz vertical geophones are used as a benchmark to evaluate the performance of the FBG accelerometer. A sledgehammer impinging on a metallic plate was used to generate shots at the two edges of the line, at 1 m from the first and last sensors. A trigger delay of 0.1 s and a 10-shot stacking was set for the standard geophone acquisition, while FBG traces were acquired continuously due to the lack of synchronization between the two systems. Similar, to the previously described lab test, the recordings were analysed using on-purpose written MATLAB codes to visualize time and frequency signal features.
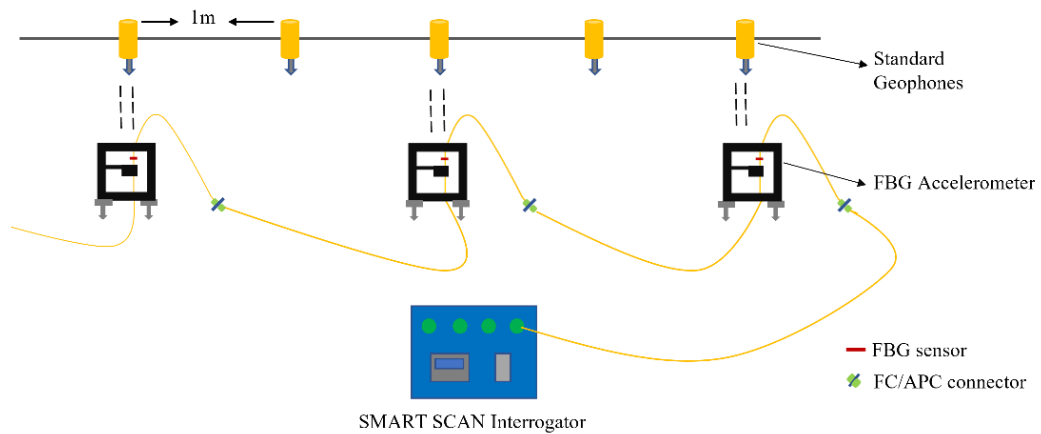
Figure 4. 11 : Schematic diagram of the field test.
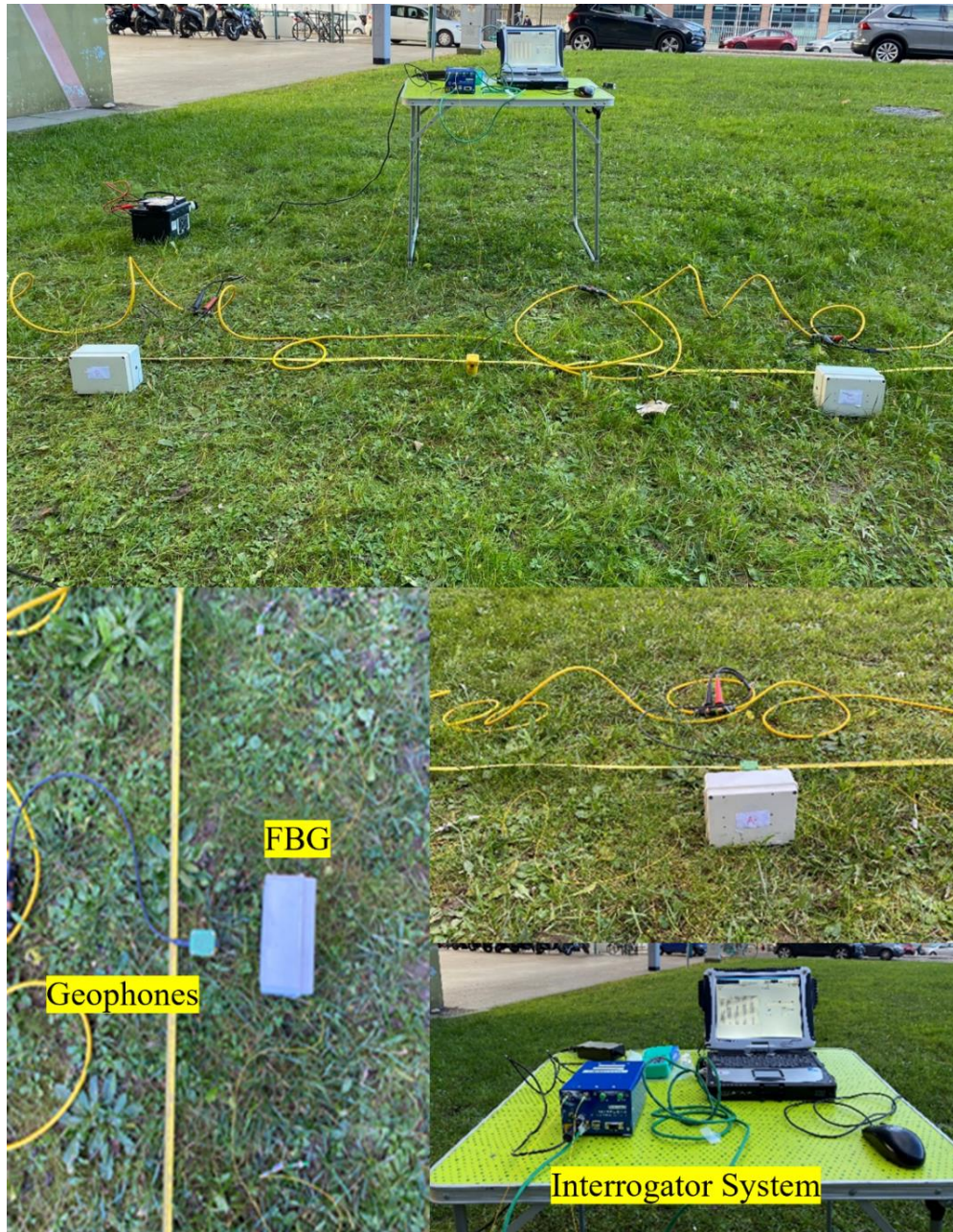
Figure 4. 12 : Field test of the calibrated system with the parallel standard geophones.

The recorded seismic traces from both instruments are shown in (*Figure 4. 13* (a and b)). Since the FBG system lacks an automatic triggering and stacking system, trace stacking to improve the signal-to-noise ratio was implemented by means of cross-correlation. In particular, the continuous FBG recordings were split into

shorter segments, roughly containing the traces related to each hammer shot. Cross-correlation between the trace closest to the source of the first shot segment and each following time segment was then undertaken. The obtained lag (delay) computed between the different time windows was then used to align the time segments and stack the traces.
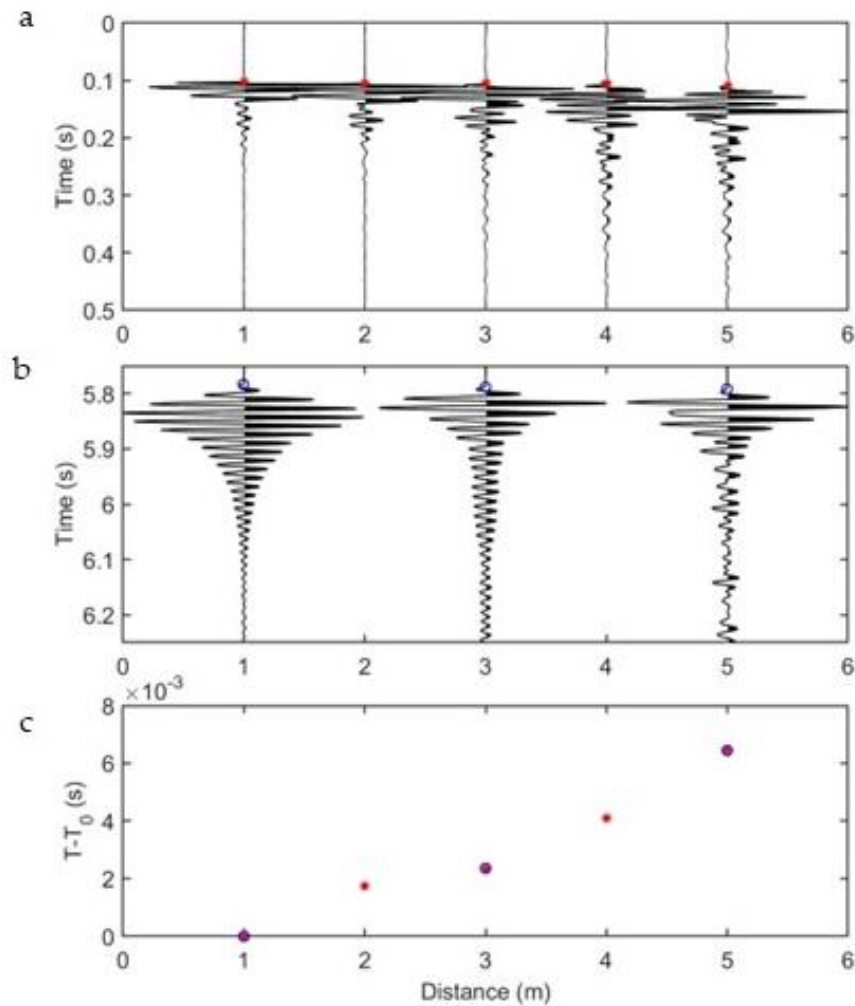
Figure 4. 13 : Seismograms of (a) standard geophones and (b) FBG accelerometer for the external hammer shots, (c) first arrival times in terms of delta T in the y-axis with respect to the sensor position of both systems.

In *Figure 4. 13*(a and b) each geophone and the FBG traces are normalized to its maximum amplitude, so no information on the attenuation of the signal amplitude can be inferred from these plots. However, the FBG sensors carry a signal with different amplitude distributions in time after the first arrival time. This is mostly due to the different amplitude in frequency bands recorded by the two sensors. However, these factors did not affect the first arrival time reading.

First arrival time picking was then carried out on the 5 stacked geophone traces and the three stacked FBG traces. Due to the missing triggering system, the time picked at the first sensor (i.e., closest to the source) was removed from both datasets. The relative arrival times at the different sensors are shown (*Figure 4. 13* (c)). The plot shows almost perfect matching between the picked travel times, demonstrating the system improvement with respect to the preliminary lab experiments.

4.5 Discussion and Conclusions

We designed and tested a simple cantilever beam based FBG accelerometer suitable for picking up the first arrival time of the active seismic source in the field. Using the already established fiber optic sensing technique, we designed, developed, fabricated, and packaged a FBG based accelerometer. For the field purpose these accelerometers are serially multiplexed and directly coupled to the ground just like standard vertical geophones. Using a single interrogator, some decades of sensors could be serially multiplexed and connected to the same fiber.

Initially, we carried out FEM simulation using ANSYS for deciding the measuring range (bandwidth) and performance, which is associated with the natural frequency of the sensor. The key parameters affecting the natural frequency of the designed sensor is the length, thickness, and breadth of the cantilever beam along with the mass block. In the simulations the breadth of the cantilever beam (20 mm) is kept fixed, and cantilever beam length (from 30 mm to 45 mm), thickness (from 1mm to 5mm) are varied to study the effects of parameters on the natural frequency. This analysis was useful to check the properties of the sensor with respect to the expected sensitivity and frequency response.

Further we calibrated the simulated design configurations in laboratory using a vibrational exciter by performing the amplitude frequency response and dynamic sensitivity test. With the help of Solid Works, the 3D model of the design was

generated and fabricated using the 3D printing technology with PLA for the laboratory calibration test. 3D printing technology was a time saver compared to other production facilities, it helped to do more customization of the system due to the fast production and the cost. The test results are found to closely matching with ANSYS modal analysis and lab calibration. The optimized FBG accelerometer (with cantilever beam parameters: total   length=60 mm, breadth =20 mm and thickness = 1mm, mass block of lead=20g) has a natural frequency of approximately 75 Hz, with an operating frequency range of 5-55 Hz, where the response remains almost flat and has a high sensitivity of ±433.7 pm/g. Overall the performance achieved for the simple and compact 3D printed proposed sensor is best for the low frequency measurements with high sensitivity .

To test these 3D printed proposed sensor in the field, we packaged this sensor inside a PVC box with two spikes attached at the bottom of the box to improve the mechanical coupling with the ground. This packaging approach make it relatively compact, lightweight, and robust for the field applications. From the field test in comparison with the 4.5 Hz vertical geophones, we observe that the first arrival time of both systems is perfectly matching. Hence, this sensor system has the potential to monitor active signals.

One of the limitations is the fragility of the FBG sensors so the installation of these sensors should be taken care well than the conventional ones which are more robust. Despite this limitation, the multiplexing capability of the FBG sensors, immunity to electromagnetic interference and the capability of the interrogation system to accommodate more sensors in one go add up to the advantage of using such systems instead of the conventional ones.

The prime objective of this work was to introduce a simple, relatively compact FBG cantilever beam-based accelerometer design with low-cost fabrication and packaging method for monitoring active signals in the field, still there is enough scope for further improvement. The advantage of this work with respect to existing designs are flexibility in reproducing and optimizing the design due to the ease of fabrication and low-cost packaging. Since we have not done the temperature compensation with a reference fiber in the system, it may fail in an operating environment with significant temperature variation. We still have room for improvement in improving the robustness of these systems and developing the triggering system for data acquisition.

Chapter 5

Conclusions

5.1 Conclusions

Since their invention, multiple parameters have been measured using fiber bragg grating sensors in a large variety of environment. In this doctoral thesis, it was proposed to research and assess the performance of Fiber Bragg Grating sensors in the engineering geophysics for the application of vibrational analysis and for non-destructive test in the structural monitoring. This chapter briefly summarizes the main results and potential directions for the future study.

Chapter 2 provides a comprehensive overview of the principles and fundamentals of fiber optic sensing with a specific focus on the Fiber Bragg Grating sensors. The section on FBG sensors delves into the detailed description on their fabrication and demodulation techniques. This chapter also provides a comprehensive overview of the applications of FBG sensors in geophysical monitoring.

In **Chapter 3** of the thesis provides an in-depth analysis of static monitoring for accessing the condition of the structure. The chapter begins by discussing about the importance and advantages of static monitoring in geophysics. This monitoring is important to understand the excessive shrinkage and the thermal gradients that can lead to cracking in the construction phase, also to optimise the material, water/cement ratio used for the construction process. The main aim of our study was to analyse the early age parameters of the two-component grout used in backfilling of tunnels. A brief overview about the two-component grout and the role of the components are discussed based on the literatures. A dual FBG sensor technique is used for the discrimination of early age strain and temperature measurements. The calibration of the temperature dual FBG sensor with the borosilicate glass capillary tube and stainless-steel tube was conducted and from the experiment it was evident that the stainless-steel tube was better.

For the investigation a bare dual FBG sensor and a dual FBG sensor encapsulated in a stainless-steel capillary tube for the temperature measurement was inserted into casting mould before the casting. The study on four different bentonite samples, a major constituent among one component was conducted for the early age shrinkage measurement for 16 days and temperature measurement mainly in the first 24 hours.

The key findings of the research are we observe an increase in the temperature of the samples in the initial hours with a slowing down due to the hydration of cement. Setting time of the samples are about 90 minutes after the casting, as this is the time at which the temperature is reached maximum. The early age temperature of the mix varies from 2 degrees to 4 degrees. We have also compared the temperature measurement of FBG sensors by embedding thermocouple before casting the sample. The measurement from both the systems were similar. From the early age analysis for 16 days from the casting. The early age shrinkage of bentonite B1 is more than other bentonites and 50 % of the shrinkage happens in the initial hours of casting then it decreases gradually and remains at a constant value at about 16 days of casting. The maximum shrinkage is for the mix B1 (about 450 $\mu\varepsilon$) while the minimum shrinkage is for the mix B4 (about 250 $\mu\varepsilon$). The difference in values of shrinkage can be due to the different used bentonite. However, it is not possible to correlate the differences found with the bentonite index considered in this research (SWI and smectite content). The difficulty in correlating the behaviour of a certain two-component grout and the used bentonite is confirmed also in the scientific literature (Todaro and Pace, 2022; Todaro et al., 2023). Analysis of the shrinkage by keeping the mix design outside the water also concludes that its losses of the natural water and mechanical properties are the reason for the excessive shrinkage.

The analysis of the shrinkage put alight the very limited magnitude of the phenomenon (< 500 $\mu\varepsilon$), abundantly within the threshold value of 10000 $\mu\varepsilon$ reported in the technical specification of some tunnel construction sites (Càmara, 2018; Todaro et al., 2022a).

From this analysis, we can conclude that all the tested mix-design are suitable for backfilling in the tunnel. This study proves FBG sensors have the potential to measure the early age parameters and static monitoring of the structures in a non-destructive way.

Chapter 4 of the thesis deals with dynamic monitoring mainly the vibrational analysis. The main aim of this study was to introduce a simple, relatively compact FBG cantilever beam-based accelerometer design with low-cost fabrication and packaging method for monitoring active signals in the field.

Initially FEM simulations using ANSYS was carried out to decide the measuring bandwidth and the performance, which is associated with the natural frequency of the sensor. The natural frequency of the sensors is affected by the parameters like length, breadth, and thickness of the cantilever beam. From the simulations we had a detailed analysis about the frequency response of different configuration of the design by varying these parameters.

Further calibration of these configured design from simulation using the vibrational exciter was carried out by performing the amplitude frequency response and dynamic sensitivity. With the help of Solid Works, the 3D model of the design was generated and fabricated using the 3D printing technology with PLA for the laboratory calibration test. 3D printing technology helped to do more customization of the system due to the fast production and the cost. The test results are found to closely matching with ANSYS modal analysis and lab calibration. The optimized FBG accelerometer (with cantilever beam parameters: total length=60 mm, breadth =20 mm and thickness = 1mm, mass block of lead=20g) has a natural frequency of approximately 75 Hz, with an operating frequency range of 5-55 Hz, where the response remains almost flat and has a high sensitivity of ±433.7 pm/g. Overall the performance achieved for the simple and relatively compact 3D printed proposed sensor is best for the low frequency measurements with high sensitivity .

To test these 3D printed proposed sensor in the field, we packaged this sensor inside a PVC box with two spikes attached at the bottom of the box to improve the mechanical coupling with the ground. This packaging approach make it relatively compact, lightweight, and robust for the field applications.

From the field test in comparison with the 4.5 Hz vertical geophones, we observe that the first arrival time of both systems is perfectly matching. Hence, this sensor system has the potential to monitor active signals.

5.2 Future Developments

This thesis demonstrates that FBG sensors are a promising sensor for the static and dynamic monitoring in the geophysics. The techniques developed in this study proves the potential use of FBG sensors for these measurements.

In the case of static monitoring there is still a room for the improvement of the packaging the FBG sensors for the temperature and strain because of the fragility of the FBG sensors, an extra care was required for the installation of the sensors into the casting mould. This can make the system more rigid and robust for the monitoring in the field.

For dynamic monitoring, since the proposed design is flexible to reproduce and optimize due to the ease of fabrication and low-cost packaging. They can be easily customized depending on our desired application based on the frequency bandwidth. Since we have not performed the temperature compensation with a reference fiber in the system, it may fail to operate in an environment with high temperature variation which can be further addressed in future studies. We still need to work on building the triggering system for data collecting and strengthening the robustness of these systems.

References

Ajo-Franklin, Jonathan B., Shan Dou, Nathaniel J. Lindsey, Inder Monga, Chris Tracy, Michelle Robertson, Veronica Rodriguez Tribaldos, et al. 2019. 'Distributed Acoustic Sensing Using Dark Fiber for Near-Surface Characterization and Broadband Seismic Event Detection'. *Scientific Reports* 9 (1): 1328. https://doi.org/10.1038/s41598-018-36675-8.

Albert, Jacques, Li-Yang Shao, and Christophe Caucheteur. 2013. 'Tilted Fiber Bragg Grating Sensors: Tilted Fiber Bragg Grating Sensors'. *Laser & Photonics Reviews* 7 (1): 83–108. https://doi.org/10.1002/lpor.201100039.

Antunes, P., Hugo Lima, Jorge Monteiro, and P. S. André. 2008. 'Elastic Constant Measurement for Standard and Photosensitive Single Mode Optical Fibres'. *Microwave and Optical Technology Letters* 50 (9): 2467–69. https://doi.org/10.1002/mop.23660.

Antunes, Paulo, Ftima Domingues, Marco Granada, and Paulo Andr. 2012. 'Mechanical Properties of Optical Fibers'. In *Selected Topics on Optical Fiber Technology*, edited by Moh. Yasin. InTech. https://doi.org/10.5772/26515.

Ashry, Islam, Yuan Mao, Biwei Wang, Frode Hveding, Ahmed Y. Bukhamsin, Tien Khee Ng, and Boon S. Ooi. 2022. 'A Review of Distributed Fiber–Optic Sensing in the Oil and Gas Industry'. *J. Lightwave Technol.* 40 (5): 1407–31.

Baldwin, Chris, Jack Niemczuk, Jason Kiddy, and Toni Salter. 2005. 'Review of Fiber Optic Accelerometers'. In *Proceedings of IMAC XXIII: A Conference & Exposition on Structural Dynamics*.

Basumallick, N., I. Chatterjee, P. Biswas, K. Dasgupta, and S. Bandyopadhyay. 2012. 'Fiber Bragg Grating Accelerometer with Enhanced Sensitivity'. *Sensors and Actuators A: Physical* 173 (1): 108–15. https://doi.org/10.1016/j.sna.2011.10.026.

Basumallick, Nandini, Palas Biswas, Kamal Dasgupta, and Somnath Bandyopadhyay. 2013. 'Design Optimization of Fiber Bragg Grating Accelerometer for Maximum Sensitivity'. *Sensors and Actuators A: Physical* 194 (May): 31–39. https://doi.org/10.1016/j.sna.2013.01.039.

Bhatia, Vikram, and Ashish M. Vengsarkar. 1996. 'Optical Fiber Long-Period Grating Sensors'. *Opt. Lett.* 21 (9): 692–94. https://doi.org/10.1364/OL.21.000692.

Campanella, Carlo, Antonello Cuccovillo, Clarissa Campanella, Abdulkadir Yurt, and Vittorio Passaro. 2018. 'Fibre Bragg Grating Based Strain Sensors: Review of Technology and Applications'. *Sensors* 18 (9): 3115. https://doi.org/10.3390/s18093115.

Casas-Ramos, Miguel A., L. Gabriela Castillo-Barrera, and G. E. Sandoval-Romero. 2018. 'Optical Accelerometer for Seismic Measurement'. *Vibroengineering PROCEDIA* 21 (December): 38–41. https://doi.org/10.21595/vp.2018.20379.

Casas-Ramos, Miguel A., and Sandoval-Romero, G.E. 2017. 'Cantilever Beam Vibration Sensor Based on the Axial Property of Fiber Bragg Grating'. *Smart Structures and Systems* 19 (6): 625–31. https://doi.org/10.12989/SSS.2017.19.6.625.

Casas-Ramos, Miguel Angel, and Gabriel Eduardo Sandoval-Romero. 2015. 'Modified Optical Fiber Bragg Grating Accelerometer'. In *2015 Argentine School of Micro-Nanoelectronics, Technology and Applications (EAMTA)*, 28–32. Villa Maria, Argentina: IEEE. https://doi.org/10.1109/EAMTA.2015.7237374.

Cavalli, Jacopo. 2018. 'EXPERIMENTAL EVALUATION OF SENSORS BASED ON FIBER BRAGG GRATING'. Polytechnic of Turin, Master's degree course in Environmental and Land Engineering, 2018. http://webthesis.biblio.polito.it/id/eprint/9120.

Chen, Jinjie, Bo Liu, and Hao Zhang. 2011. 'Review of Fiber Bragg Grating Sensor Technology'. *Frontiers of Optoelectronics in China* 4: 204–12.

Costa Antunes, P.F. da, H.F.T. Lima, N.J. Alberto, H. Rodrigues, P.M.F. Pinto, J. de Lemos Pinto, R.N. Nogueira, H. Varum, A.G. Costa, and P.S. de Brito Andre. 2009. 'Optical Fiber Accelerometer System for Structural Dynamic Monitoring'. *IEEE Sensors Journal* 9 (11): 1347–54. https://doi.org/10.1109/JSEN.2009.2026548.

Dewra, Sanjeev, and Amit Grover. 2015. 'Fabrication and Applications of Fiber Bragg Grating-a Review'. *Advanced Engineering Technology and Application* 4 (3): 7–17.

Dingyi Feng, Xueguang Qiao, Hangzhou Yang, Qiangzhou Rong, Ruohui Wang, Yanying Du, Manli Hu, and Zhongyao Feng. 2015. 'A Fiber Bragg Grating Accelerometer Based on a Hybridization of Cantilever Beam'. *IEEE Sensors Journal* 15 (3): 1532–37. https://doi.org/10.1109/JSEN.2014.2364122.

Dong, Xiaoyi, Hao Zhang, Bo Liu, and Yinping Miao. 2011. 'Tilted Fiber Bragg Gratings: Principle and Sensing Applications'. *Photonic Sensors* 1 (1): 6–30. https://doi.org/10.1007/s13320-010-0016-x.

Doyle, Crispin. 2003. 'Fibre Bragg Grating Sensors-an Introduction to Bragg Gratings and Interrogation Techniques'. *Smart Fibres Ltd* 1: 1–5.

Dragomir, Claudiu Sorin, and Daniela Dobre. 2021. 'From Seismic Instrumentation Towards Disaster Prevention and Mitigation'. *IOP Conference Series: Materials Science and Engineering* 1203 (3): 032090. https://doi.org/10.1088/1757-899X/1203/3/032090.

E., Dal Negro. October. 'Two-Component Backfill Grout System in TBM. The Experience of the Tunnel "Sparvo" in Italy, In'. In *Proceedings of the Tunnelling in a Resource Driven World Conference, 2014, TAC*, 26–28. Vancouver, CA.

EFNARC. 2005. 'Specification and Guidelines for the Use of Specialist Products for Mechanised Tunnelling (TBM) in Soft Ground and Hard Rock'.

Eid, Mahmoud M. A. 2022. 'Optical Fiber Sensors: Review of Technology and Applications'. *Indonesian Journal of Electrical Engineering and Computer Science* 25 (2): 1038. https://doi.org/10.11591/ijeecs.v25.i2.pp1038-1046.

Elies, Stephan. 2015. 'Performance Analysis of Commercial Accelerometers: A Parameter Review'. *Sensors & Transducers* 193 (10): 179.

Enrico, DAL NEGRO, Alessandro BOSCARO, Richard SCHULKINS, and Gianluca GULINO. 2010. 'Two-Component Backfill Grouting on Rome's Line C'. *Progressive Media Group, Sidcup*, pp 45-48, 4 p.

Fenta, Mulugeta C., David K. Potter, and János Szanyi. 2021a. 'Fibre Optic Methods of Prospecting: A Comprehensive and Modern Branch of Geophysics'. *Surveys in Geophysics* 42 (3): 551–84. https://doi.org/10.1007/s10712-021-09634-8.

———. 2021b. 'Fibre Optic Methods of Prospecting: A Comprehensive and Modern Branch of Geophysics'. *Surveys in Geophysics* 42 (3): 551–84. https://doi.org/10.1007/s10712-021-09634-8.

Fidanboylu, Kemal, and H. S. Efendioglu. 2009. 'Fiber Optic Sensors and Their Applications'. In *5th International Advanced Technologies Symposium (IATS'09)*, 6:2–3.

Gangopadhyay, Tarun Kumar. 2004. 'Prospects for Fibre Bragg Gratings and Fabry-Perot Interferometers in Fibre-Optic Vibration Sensing'. *Sensors and Actuators A: Physical* 113 (1): 20–38. https://doi.org/10.1016/j.sna.2004.01.043.

García, Yoany Rodríguez, Jesús M. Corres, and Javier Goicoechea. 2010. 'Vibration Detection Using Optical Fiber Sensors'. Edited by Ignacio Matias. *Journal of Sensors* 2010 (September): 936487. https://doi.org/10.1155/2010/936487.

Guo, Teng, Tianxi Zhang, Yizhuo Li, and Xueguang Qiao. 2020. 'Highly Sensitive FBG Seismometer With a 3D-Printed Hexagonal Configuration'. *Journal of Lightwave Technology* 38 (16): 4588–95. https://doi.org/10.1109/JLT.2020.2991667.

Guo, Yongxing, Min Chen, Li Xiong, Xinglin Zhou, and Cong Li. 2021. 'Fiber Bragg Grating Based Acceleration Sensors: A Review'. *Sensor Review* 41 (1): 101–22. https://doi.org/10.1108/SR-10-2020-0243.

Hafizi, Z M, and E Vorathin. 2021a. 'Investigation of Low Frequency Fibre Bragg Grating Accelerometer Based on Thermoplastic Cantilever Beam'. *IOP Conference Series: Materials Science and Engineering* 1078 (1): 012012. https://doi.org/10.1088/1757-899X/1078/1/012012.

———. 2021b. 'Investigation of Low Frequency Fibre Bragg Grating Accelerometer Based on Thermoplastic Cantilever Beam'. *IOP Conference Series: Materials Science and Engineering* 1078 (1): 012012. https://doi.org/10.1088/1757-899X/1078/1/012012.

He, Siyue, Jinxing Lai, Lixin Wang, and Ke Wang. 2020. 'A Literature Review on Properties and Applications of Grouts for Shield Tunnel'. *Construction and Building Materials* 239 (April): 117782. https://doi.org/10.1016/j.conbuildmat.2019.117782.

He, Zuyuan, and Qingwen Liu. 2021. 'Optical Fiber Distributed Acoustic Sensors: A Review'. *J. Lightwave Technol.* 39 (12): 3671–86. https://doi.org/10.1364/JLT.39.003671.

Hill, K. O., Y. Fujii, D. C. Johnson, and B. S. Kawasaki. 1978. 'Photosensitivity in Optical Fiber Waveguides: Application to Reflection Filter Fabrication'. *Applied Physics Letters* 32 (10): 647–49. https://doi.org/10.1063/1.89881.

Hill, K.O., and G. Meltz. 1997. 'Fiber Bragg Grating Technology Fundamentals and Overview'. *Journal of Lightwave Technology* 15 (8): 1263–76. https://doi.org/10.1109/50.618320.

Hong, Li, Rui Sun, Zhongchao Qiu, Zhiming Han, and Yanan Li. 2021. 'A Multi-Cantilever Beam Low-Frequency FBG Acceleration Sensor'. *Scientific Reports* 11 (1): 18502. https://doi.org/10.1038/s41598-021-98055-z.

Jiang, Nuan, Hai Zhu, Kai Bao, and Yongming Hu. 2015. 'Simultaneous Discrimination of Strain and Temperature Using Dual-Gratings in One Fiber'. *Optik* 126 (23): 3974–77. https://doi.org/10.1016/j.ijleo.2015.07.179.

Kadhum Hisham, Hisham. 2018. 'Optical Fiber Sensing Technology: Basics, Classifications and Applications'. *American Journal of Remote Sensing* 6 (1): 1. https://doi.org/10.11648/j.ajrs.20180601.11.

Li, Tianliang, Jinxiu Guo, Yuegang Tan, and Zude Zhou. 2020. 'Recent Advances and Tendency in Fiber Bragg Grating-Based Vibration Sensor: A Review'.

IEEE Sensors Journal 20 (20): 12074–87. https://doi.org/10.1109/JSEN.2020.3000257.

Li, Zefeng. 2021. 'Recent Advances in Earthquake Monitoring I: Ongoing Revolution of Seismic Instrumentation'. *Earthquake Science* 34 (2): 177–88. https://doi.org/10.29382/eqs-2021-0011.

Lindsey, Nathaniel J., and Eileen R. Martin. 2021. 'Fiber-Optic Seismology'. *Annual Review of Earth and Planetary Sciences* 49 (1): 309–36. https://doi.org/10.1146/annurev-earth-072420-065213.

Luo, Dong, Zubaidah Ismail, and Zainah Ibrahim. 2013. 'Added Advantages in Using a Fiber Bragg Grating Sensor in the Determination of Early Age Setting Time for Cement Pastes'. *Measurement* 46 (10): 4313–20. https://doi.org/10.1016/j.measurement.2013.06.036.

M. Reynolds, John. n.d. *An Introduction to Applied and Environmental Geophysics*.

Mamidi, Venkata Reddy, Srimannarayana Kamineni, L. N. Sai Prasad Ravinuthala, Venkatapparao Thumu, and Vengal Rao Pachava. 2014. 'Characterization of Encapsulating Materials for Fiber Bragg Grating-Based Temperature Sensors'. *Fiber and Integrated Optics* 33 (4): 325–35. https://doi.org/10.1080/01468030.2014.932472.

Meltz, G., W. W. Morey, and W. H. Glenn. 1989. 'Formation of Bragg Gratings in Optical Fibers by a Transverse Holographic Method'. *Opt. Lett.* 14 (15): 823–25. https://doi.org/10.1364/OL.14.000823.

Mesboua, Noureddine, Khaled Benyounes, and Abdelbaki Benmounah. 2018. 'Study of the Impact of Bentonite on the Physico-Mechanical and Flow Properties of Cement Grout'. Edited by Sanjay Kumar Shukla. *Cogent Engineering* 5 (1): 1446252. https://doi.org/10.1080/23311916.2018.1446252.

Pei, Huafu, Zongjin Li, Bo Zhang, and Hongyan Ma. 2014. 'Multipoint Measurement of Early Age Shrinkage in Low w/c Ratio Mortars by Using Fiber Bragg Gratings'. *Materials Letters* 131 (September): 370–72. https://doi.org/10.1016/j.matlet.2014.05.202.

Peila, Daniele, Luca Borio, and Sebastiano Pelizza. 2011. 'The Behaviour of a Two-Componenet Back-Filling Grout Used in a Tunnel-Boring Machine'. *Acta Geotechnica Slovenica* 8 (1): 5–15.

Pendão, Cristiano, and Ivo Silva. 2022. 'Optical Fiber Sensors and Sensing Networks: Overview of the Main Principles and Applications'. *Sensors* 22 (19): 7554. https://doi.org/10.3390/s22197554.

Rao, Yun-Jiang, Zeng-Ling Ran, and Yuan Gong. 2017. *Fiber-Optic Fabry–Perot Sensors: An Introduction*. 1st ed. Boca Raton, FL : CRC Press, Taylor & Francis Group, [2017]: CRC Press. https://doi.org/10.1201/9781315120997.

Reghuprasad, Aarathy Ezhuthupally, Chiara Colombero, and Alberto Godio. 2023. 'Serially Connected Cantilever Beam-Based FBG Accelerometers: Design, Optimization and Testing'. *Sensors* 23 (6): 3188. https://doi.org/10.3390/s23063188.

Riza, Muhammad Arif, Yun Ii Go, Sulaiman Wadi Harun, and Robert R. J. Maier. 2020. 'FBG Sensors for Environmental and Biochemical Applications—A Review'. *IEEE Sensors Journal* 20 (14): 7614–27. https://doi.org/10.1109/JSEN.2020.2982446.

Sabri, Naseer, S A Aljunid, M S Salim, R B Ahmad, and R Kamaruddin. 2013. 'Toward Optical Sensors: Review and Applications'. *Journal of Physics: Conference Series* 423 (April): 012064. https://doi.org/10.1088/1742-6596/423/1/012064.

Safiuddin, Md., A. Kaish, Chin-Ong Woon, and Sudharshan Raman. 2018. 'Early-Age Cracking in Concrete: Causes, Consequences, Remedial Measures, and Recommendations'. *Applied Sciences* 8 (10): 1730. https://doi.org/10.3390/app8101730.

Scudero, Salvatore, Antonino D'Alessandro, Luca Greco, and Giovanni Vitale. 2018. 'MEMS Technology in Seismology: A Short Review'. In *2018 IEEE International Conference on Environmental Engineering (EE)*, 1–5. Milan: IEEE. https://doi.org/10.1109/EE1.2018.8385252.

Shang, Ying, Maocheng Sun, Chen Wang, Jian Yang, Yuankai Du, Jichao Yi, Wenan Zhao, Yingying Wang, Yanjie Zhao, and Jiasheng Ni. 2022. 'Research Progress in Distributed Acoustic Sensing Techniques'. *Sensors* 22 (16): 6060. https://doi.org/10.3390/s22166060.

Silkina, Tatiana. 2014. 'Application of Distributed Acoustic Sensing to Flow Regime Classification'. In .

Slowik, Volker, Evelyn Schlattner, and Thomas Klink. 2004. 'Experimental Investigation into Early Age Shrinkage of Cement Paste by Using Fibre Bragg Gratings'. *Cement and Concrete Composites* 26 (5): 473–79. https://doi.org/10.1016/S0958-9465(03)00077-5.

Sotnik, Svitlana, and Vyacheslav Lyashenko. 2022. 'Overview of Modern Accelerometers'.

Srimannarayana, Kamineni, Madhuvarasu Shankar, Ravinuthala Prasad, T.K. Mohan, Ramakrishna S, Srikanth G, and Sriramoju Rao. 2008. 'Fiber Bragg Grating and Long Period Grating Sensor for Simultaneous Measurement and Discrimination of Strain and Temperature Effects'. *Optica Applicata* 38 (January).

Todaro, Carmine, and Francesca Pace. 2022a. 'Elastic Properties of Two-Component Grouts at Short Curing Times: The Role of Bentonite'. *Tunnelling*

and Underground Space Technology 130 (December): 104756. https://doi.org/10.1016/j.tust.2022.104756.

———. 2022b. 'Elastic Properties of Two-Component Grouts at Short Curing Times: The Role of Bentonite'. *Tunnelling and Underground Space Technology* 130 (December): 104756. https://doi.org/10.1016/j.tust.2022.104756.

Todaro, Carmine, Simone Saltarin, and Marilena Cardu. 2022a. 'Bentonite in Two-Component Grout Applications'. *Case Studies in Construction Materials* 16 (June): e00901. https://doi.org/10.1016/j.cscm.2022.e00901.

———. 2022b. 'Bentonite in Two-Component Grout Applications'. *Case Studies in Construction Materials* 16 (June): e00901. https://doi.org/10.1016/j.cscm.2022.e00901.

Tosi, Daniele. 2018. 'Review of Chirped Fiber Bragg Grating (CFBG) Fiber-Optic Sensors and Their Applications'. *Sensors* 18 (7): 2147. https://doi.org/10.3390/s18072147.

Tyler, S.W., D.M. Holland, V. Zagorodnov, A.A. Stern, C. Sladek, S. Kobs, S. White, F. Suárez, and J. Bryenton. 2013. 'Using Distributed Temperature Sensors to Monitor an Antarctic Ice Shelf and Sub-Ice-Shelf Cavity'. *Journal of Glaciology* 59 (215): 583–91. https://doi.org/10.3189/2013JoG12J207.

Ukil, Abhisek, Hubert Braendle, and Peter Krippner. 2012. 'Distributed Temperature Sensing: Review of Technology and Applications'. *IEEE Sensors Journal* 12 (5): 885–92. https://doi.org/10.1109/JSEN.2011.2162060.

Weng, Yinyan, Xueguang Qiao, Tuan Guo, Manli Hu, Zhongyao Feng, Ruohui Wang, and Jing Zhang. 2012. 'A Robust and Compact Fiber Bragg Grating Vibration Sensor for Seismic Measurement'. *IEEE Sensors Journal* 12 (4): 800–804. https://doi.org/10.1109/JSEN.2011.2166258.

Wong, Allan C.L., Paul A. Childs, Richard Berndt, Tony Macken, Gang-Ding Peng, and Nadarajah Gowripalan. 2007. 'Simultaneous Measurement of Shrinkage and Temperature of Reactive Powder Concrete at Early-Age Using Fibre Bragg Grating Sensors'. *Cement and Concrete Composites* 29 (6): 490–97. https://doi.org/10.1016/j.cemconcomp.2007.02.003.

Wu, Jack, Vlastimil Masek, and Michael Cada. 2009. 'The Possible Use of Fiber Bragg Grating Based Accelerometers for Seismic Measurements'. In *2009 Canadian Conference on Electrical and Computer Engineering*, 860–63. St. John's, NL, Canada: IEEE. https://doi.org/10.1109/CCECE.2009.5090251.

Yinyan Weng, 翁银燕, 乔学光 Xueguang Qiao, 冯忠耀 Zhongyao Feng, 忽满利 Manli Hu, 张敬花 Jinghua Zhang, and 杨杨 Yang Yang. 2011. 'Compact FBG Diaphragm Accelerometer Based on L-Shaped Rigid Cantilever Beam'.

Chinese Optics Letters 9 (10): 100604–7. https://doi.org/10.3788/COL201109.100604.

Zhang, Xiaolei, Qiangzhou Rong, Hao Sun, Shen Yang, Liutong Yuan, and Manli Hu. 2014. 'Low-Frequency Fiber Bragg Grating Accelerometer Based on a Double-Semicircle Cantilever'. *Optical Fiber Technology* 20 (3): 190–93. https://doi.org/10.1016/j.yofte.2014.01.006.

Zhu, Chen, Hongkun Zheng, Lingmei Ma, Zheyi Yao, Bo Liu, Jie Huang, and Yunjiang Rao. 2023. 'Advances in Fiber-Optic Extrinsic Fabry-Perot Interferometric Physical and Mechanical Sensors: A Review'. *IEEE Sensors Journal*, 1–1. https://doi.org/10.1109/JSEN.2023.3244820.

Zhu, Hong-Hu, Bin Shi, and Cheng-Cheng Zhang. 2017. 'FBG-Based Monitoring of Geohazards: Current Status and Trends'. *Sensors* 17 (3): 452. https://doi.org/10.3390/s17030452.